NASA TECHNICAL NOTE

NASA TN D-6087

NASA TN D-6087

SIMULATION AND ANALYSIS OF PANEL SEPARATION FROM THE APOLLO 13 SERVICE MODULE

by H. Wayne Leonard, Martin M. Mikulas, Jr.,
Homer G. Morgan, and William R. Cofer

Langley Research Center
Hampton, Va. 23365

1. Report No. NASA TN D-6087	2. Government Accession No.	3. Recipient's Catalog No.
4. Title and Subtitle SIMULATION AND ANALYSIS OF PANEL SEPARATION FROM THE APOLLO 13 SERVICE MODULE		5. Report Date December 1970
		6. Performing Organization Code
7. Author(s) H. Wayne Leonard, Martin M. Mikulas, Jr., Homer G. Morgan, and William R. Cofer		8. Performing Organization Report No. L-7426
9. Performing Organization Name and Address NASA Langley Research Center Hampton, Va. 23365		10. Work Unit No. 124-08-14-08
		11. Contract or Grant No.
12. Sponsoring Agency Name and Address National Aeronautics and Space Administration Washington, D.C. 20546		13. Type of Report and Period Covered Technical Note
		14. Sponsoring Agency Code

15. Supplementary Notes

16. Abstract

An experimental and analytical program was conducted to simulate the separation of the service module bay 4 cover panel from the Apollo 13 spacecraft which occurred during its flight accident. The study was also intended to establish failure mechanisms, pressure distributions, and pressure time histories that would explain the essentially complete separation that was observed in the photographs taken by the Apollo 13 crew.

Complete separations of both isotropic and sandwich one-half-scale panel models from a boilerplate test fixture were achieved by rapidly pressurizing the oxygen shelf space with air in a vacuum environment. The sandwich panels tested were most representative of flight hardware. One particular sandwich panel separated as a result of a nonuniform pressure distribution of over 40 psi in the oxygen shelf space 20 milliseconds after start of pressurization; this result was the one most nearly consistent with known flight events. A similar test at slightly lower pressure did not separate the panel; thus, the separation pressure distribution and time history boundary was established.

17. Key Words (Suggested by Author(s)) Apollo Structural mechanics Pressurization Dynamic models	18. Distribution Statement Unclassified – Unlimited		
19. Security Classif. (of this report) Unclassified	20. Security Classif. (of this page) Unclassified	21. No. of Pages 61	22. Price* $3.00

CONTENTS

SIMULATION AND ANALYSIS OF PANEL SEPARATION
FROM THE APOLLO 13 SERVICE MODULE

By H. Wayne Leonard, Martin M. Mikulas, Jr.,
Homer G. Morgan, and William R. Cofer
Langley Research Center

SUMMARY

An experimental and analytical program was conducted to simulate the separation of the service module bay 4 cover panel from the Apollo 13 spacecraft which occurred during its flight accident. The study was also intended to establish failure mechanisms, pressure distributions, and pressure time histories that would explain the essentially complete separation that was observed in the photographs taken by the Apollo 13 crew.

One-half-scale dynamic models of the cover panel were tested on a boilerplate test fixture that simulated the internal free volume and venting of the service module. Both isotropic and sandwich panel models were studied, and tests were conducted in atmosphere and in a vacuum chamber. Panel loadings were provided by a pressurization system that rapidly released air into the oxygen shelf space of the service module bay 4 at the location of the number 2 oxygen tank. Both static and dynamic structural analyses were conducted in support of the tests.

Complete separations of both isotropic and sandwich one-half-scale panel models from the test fixture were achieved in a vacuum environment. However, the sandwich panel tests were most representative of flight conditions. One particular sandwich panel separated as a result of a nonuniform pressure distribution with peak pressures of over 40 psi in the oxygen shelf space 20 milliseconds after start of pressurization (40 milliseconds full scale); this result was the one most nearly consistent with known flight events. A similar test at slightly lower pressure failed to separate a panel and indicated that the separation boundary for this pressure distribution and time history had been established.

I. INTRODUCTION

During the Apollo 13 mission, an anomaly occurred in the service module (SM) section of the spacecraft that resulted in extensive vehicle damage and abort of the mission. A review board investigated all phases of the anomaly and reported its findings in reference 1. The study reported herein was conducted at the NASA Langley Research Center to answer questions of the review board concerning one phase of the anomaly.

The Langley study was initiated when photographs taken by the Apollo 13 crew (fig. I-1 and ref. 1) indicated that the service module bay 4 cover panel was almost completely missing after the incident with only small fragments of the panel still attached to the vehicle. The objective of the present study was to demonstrate complete separation of the panel from the spacecraft in a manner consistent with known flight events. Since only limited indirect evidence existed on the nature of input forces that caused separation, the failure mechanism and pressure loading leading to separation were also to be determined.

The experimental and analytical investigation of panel separation described herein used one-half-scale dynamic models of the service module bay 4 cover panel. Panels were tested on a fixture with scaled service module geometry and volume. Separation was simulated both in atmosphere and in a vacuum chamber by rapidly pressurizing the test fixture with air.

Numerous people at the Langley Research Center contributed to this interdisciplinary study. Although chapters of this report have been prepared by the individuals most knowledgeable about that particular phase of the program, both the report and the study were team efforts.
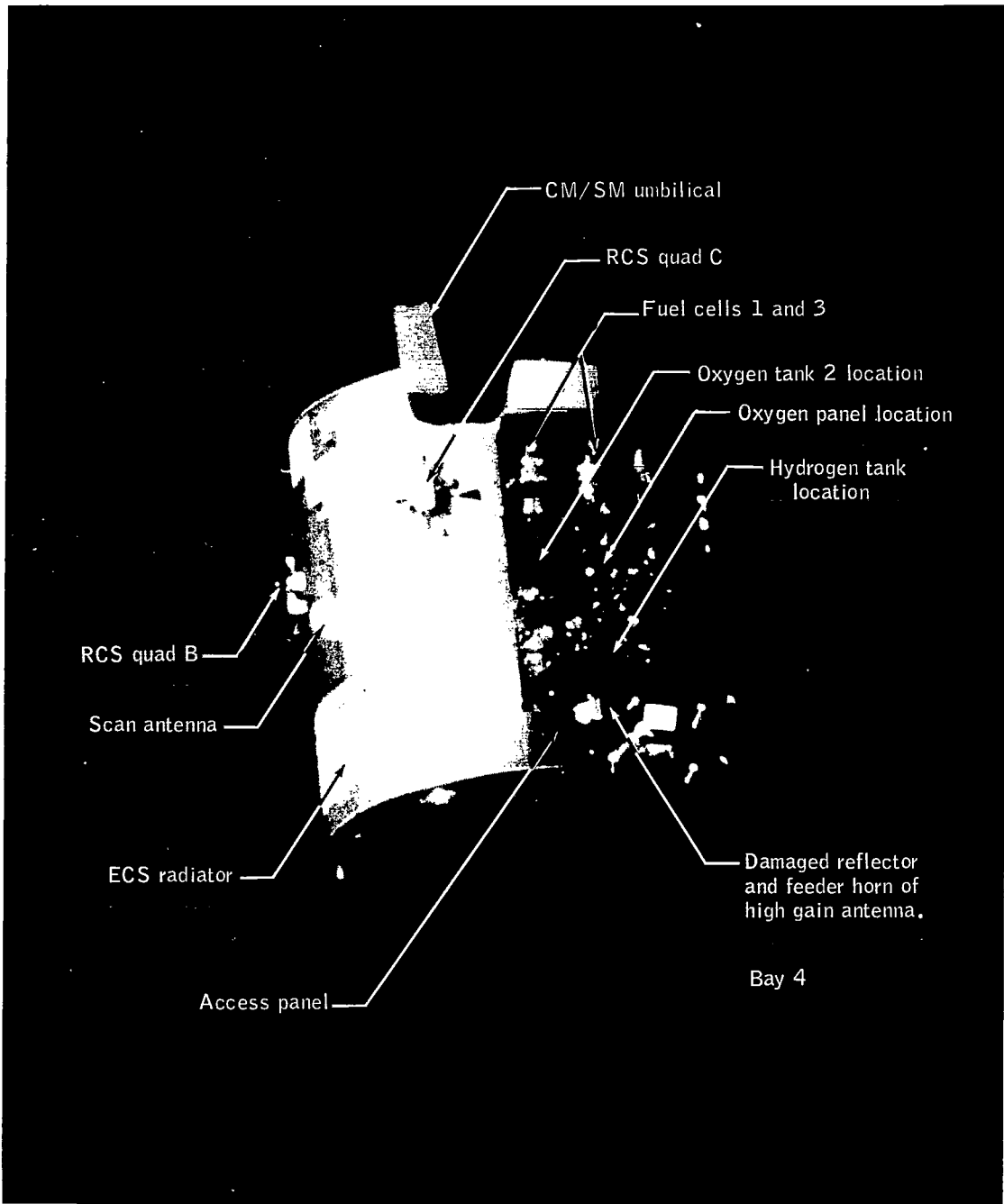
Symbols

A	area
A_n	area of nth orifice
A_L	effective air-leakage area
d	diameter
E	modulus of elasticity
EI	bending stiffness
I	moment of inertia

l	length
m	mass
N_{max}	maximum edge load
p	pressure
p_o	reference pressure
Δp	pressure increment
R	gas constant; also radius of panel
s	stress
T	absolute temperature
t	time
V	volume
V_n	volume of nth space
v	velocity
W_L	air-leakage weight flow rate
W_n	weight flow rate through nth orifice
ν	Poisson's ratio
ρ	material density
ρ_c	density of core material
ρ_s	density of face sheet material

Subscripts:

i	initial
f	full scale
m	model

CM/SM umbilical

RCS quad C

Fuel cells 1 and 3

Oxygen tank 2 location

Oxygen panel location

Hydrogen tank location

RCS quad B

Scan antenna

ECS radiator

Access panel

Damaged reflector and feeder horn of high gain antenna.

Bay 4

L-70-4774

Figure I-1.- In-flight photograph of Apollo 13 service module showing damage to bay 4.
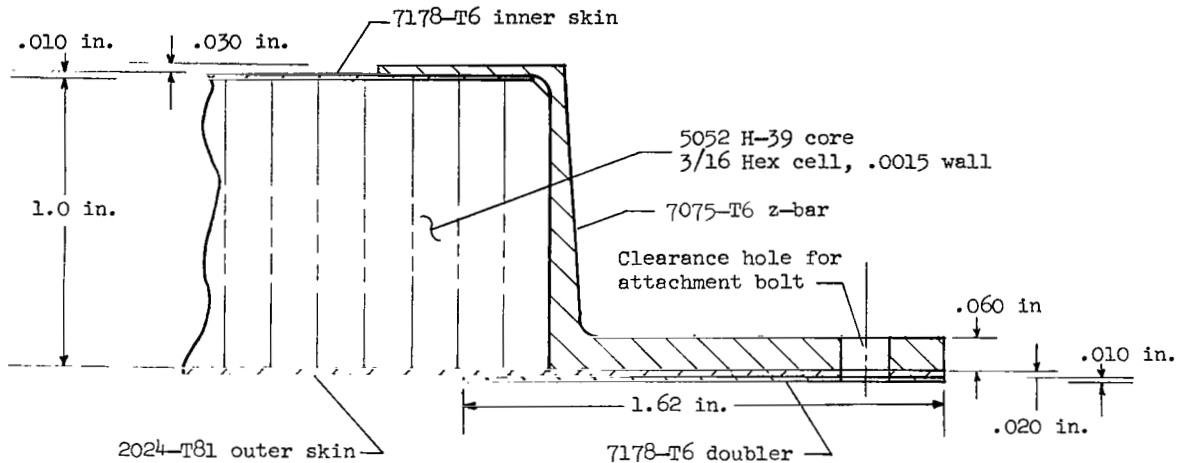
II. DYNAMIC MODELS

By H. Wayne Leonard and John C. Gustafson
Langley Research Center

Full-Scale Panel

The cover panel is a shallow cylindrical honeycomb sandwich structure with aluminum face sheets. Edge closeout is accomplished through an aluminum z-bar bonded to the face sheets and to the core material, as shown in sketch II(a). Inner-face-sheet

Sketch II(a).- Full-scale-panel edge closure.

tensile loads are transmitted to the z-bar outer flange through shear in the peripheral section of the honeycomb core which is densified in this region to carry the loads. Doublers are bonded to the external surfaces of both face sheets in critical areas such as those near the panel edges, over skin splices, and cutout areas. A 21.8×21.8-inch access door is framed into the panel at the lower left corner. Cylindrical inserts in the panel face are provided for bolting through to the internal shelf faces. The panel is attached to the service module by bolts which pass through clearance holes in the outer z-bar flange, through slightly larger clearance holes in a flange or cap at the edge of the service module radial beam, and then into nut plates attached to the inner surface of this cap. The ends of the cover panel are similarly attached to the forward and aft service module bulkheads.

Approach

The one-half-scale models of the Apollo service module bay 4 and its cover panel were practical and economical tools for determination of the internal pressure loadings required to effect total separation of the panel from the spacecraft and for definition of

the structural failure mechanism in the panel as a consequence of these loadings. In the ideal case, the model would be a perfect subscale replica of the full-scale structure. However, engineering judgment and economic considerations led to certain simplifications in the models. Initial tests were conducted on isotropic panels that scaled only membrane properties. These models were based on the assumption that panel resistance to off-design internal pressure loading such as occurred during the Apollo 13 incident would be membrane in nature in spite of very high local bending stiffness. More completely scaled sandwich panels were studied later in the program.

Scaling

The adoption of direct geometric scaling with a ratio of 1:2 and the use of similar materials between full scale and model (denoted by subscripts f and m, respectively) dictate the following model to full-scale relationships:

Parameter	Ratio	Scale value
Length, l	l_m/l_f	1/2
Diameter, d	d_m/d_f	1/2
Time, t	t_m/t_f	1/2
Velocity, v	v_m/v_f	1
Area, A	A_m/A_f	1/4
Volume, V	V_m/V_f	1/8
Mass, m	m_m/m_f	1/8
Bending stiffness, EI	$(EI)_m/(EI)_f$	1/16
Modulus of elasticity, E	E_m/E_f	1
Poisson's ratio, ν	ν_m/ν_f	1
Material density, ρ	ρ_m/ρ_f	1
Pressure, p	p_m/p_f	1
Stress, s	s_m/s_f	1

Isotropic Panel Models

The simplified isotropic panels used in the initial phases of the test program are illustrated in sketch II(b) and were designed to scale only the nominal tensile strength of
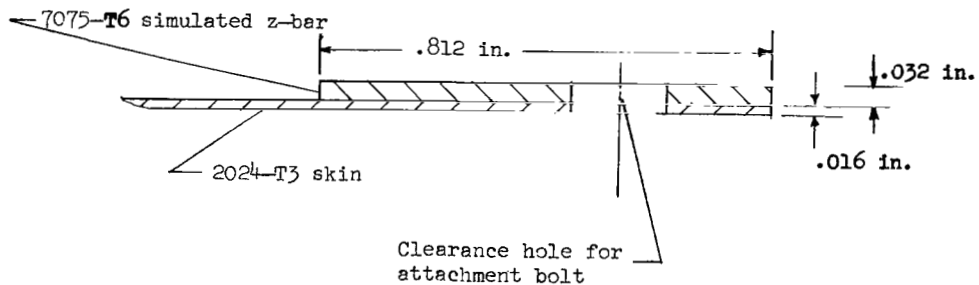
Sketch II(b).- Isotropic panel edge closure.

the full-scale panel. This approach was based on the assumption that the panel would behave essentially as a membrane during pressurization and initial failure. A single face sheet, designed to yield the scaled cumulative tensile strength of the two full-scale face sheets, was bonded to a flat edge bar which was scaled to represent the outer flange of the z-bar closeout. Doublers and hole patterns for both edge and shelf bolts were also provided. External and bolt pattern dimensions are identical to those shown for the sandwich panel in figure II-1.
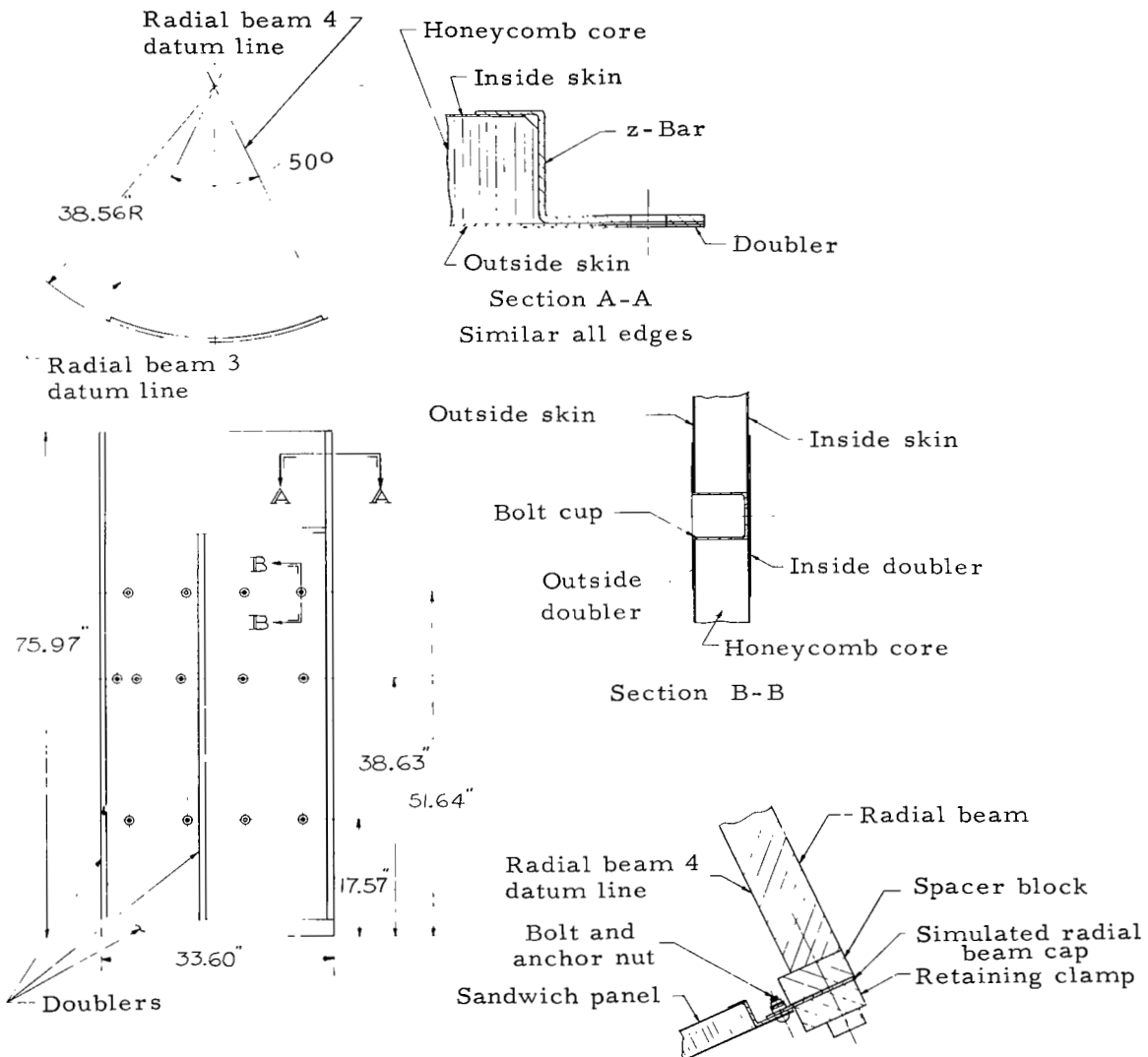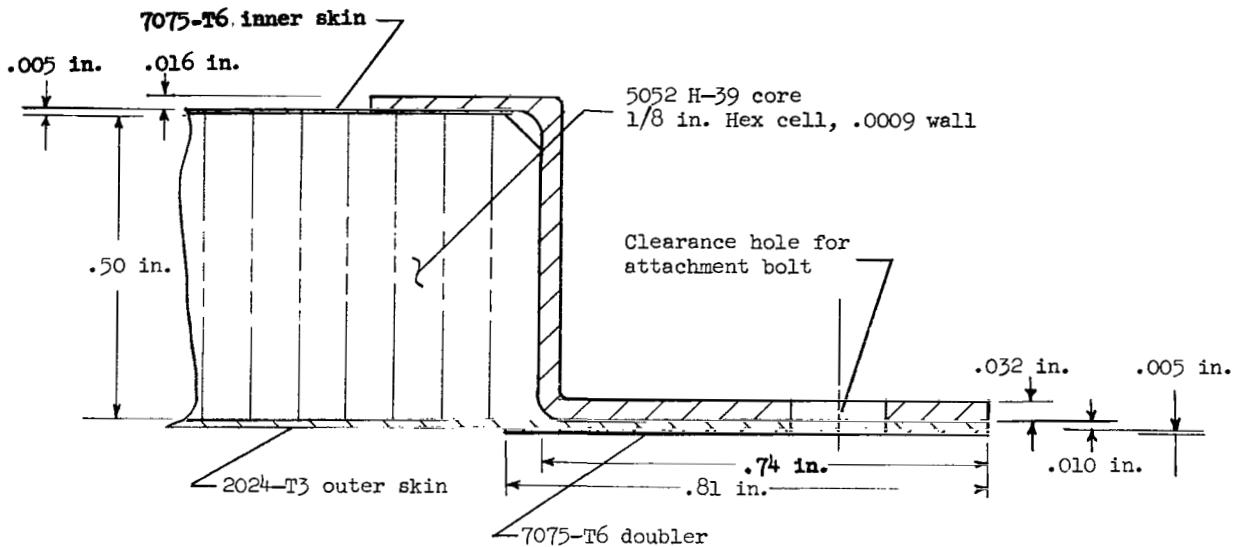

Figure II-1.- One-half-scale sandwich panel configuration.

Sandwich Panel Models

The philosophy which governed the design and fabrication of the one-half-scale honeycomb sandwich panel shown in sketch II(c) and in figure II-1 was to obtain as close to replica reproduction of the full-scale panel as was possible within the constraints of

Sketch II(c).- Half-scale sandwich-panel edge closure.

time and available materials. The fidelity of the model panels is illustrated in table II-I which lists full-scale, true half-scale, and actual model properties. It is felt that the resulting sandwich models were adequate representations of the full-scale panels and that the data derived from the test program can be interpreted in terms of full-scale panel behavior.

Honeycomb core.- The honeycomb core for the sandwich panels was 5052 aluminum with a 0.125-inch hexagonal cell and a nominal density of 3.1 pounds per cubic foot. The first two panels were fabricated with unvented material whereas vented honeycomb was used in the other panels. A densification filler composed of 80-percent microballoons and 20-percent EPON 828 epoxy resin was cured into the areas around the periphery of the panels and in the area immediately adjacent to the shelf-panel bolt fittings. This procedure was used to simulate the densified honeycomb used in the same areas of the flight panel.

Face sheets.- The outer skin was made from 0.010-inch thick 2024-T3 aluminum sheet whereas the inner skin was 0.005-inch-thick 7075-T6 aluminum. Chem-milling was required to yield these nominal half-scale values. The inner skin was chem-milled from 0.016-inch-thick sheet.

TABLE II-I

SANDWICH MODEL AND FULL-SCALE COMPONENT COMPARISON

Component	Full scale		Required for replica scaling		Actual model values	
	Material	Physical properties	Material	Physical properties	Material	Physical properties
Outer face sheet	Aluminum 2024-T81	Length . . . . 151.94 in. Width . . . . 67.04 in. Thickness . . . . 0.020 in. Ultimate tensile strength (typical) . . . . 70 ksi	Aluminum 2024-T81	Length . . . . 75.97 in. Width . . . . 33.52 in. Thickness . . . . 0.010 in. Ultimate tensile strength . . . 70 ksi	Aluminum 2024-T3	Length . . . . 75.97 in. Width . . . . 33.60 in. Thickness . . . . 0.010 in. Ultimate tensile strength . . . 70 ksi
Inner face sheet	Aluminum 7178-T6	Length . . . . 149.15 in. Width . . . . 63.00 in. Thickness . . . . 0.010 in. Ultimate tensile strength (typical) . . . . 88 ksi	Aluminum 7178-T6	Length . . . . 74.58 in. Width . . . . 31.50 in. Thickness . . . . 0.005 in. Ultimate tensile strength . . . 88 ksi	Aluminum 7075-T6	Length . . . . 74.58 in. Width . . . . 31.58 in. Thickness (av) . . . . 0.0053 in. Ultimate tensile strength . . . 83 ksi
Honeycomb core (center areas)	Aluminum 5052-H39	Cell size . . . . 3/16 in. hex. Wall thickness . . . . 0.0007 in. Core depth . . . . 0.992 in. Density . . . . 2.2 lb/ft^3	Aluminum 5052-H39	Cell size . . . . 3/32 in. hex. Wall thickness . . . . 0.00035 in. Core depth . . . . 0.496 in. Density . . . . 2.2 lb/ft^3	Aluminum 5052-H39	Cell size . . . . 1/8 in. hex. Wall thickness . . . . 0.0009 in. Core depth . . . . 0.500 in. Density . . . . 3.1 lb/ft^3
Honeycomb core (densified areas)	Aluminum 5052-H39	Cell size . . . . 3/16 in. hex. Wall thickness . . . . 0.0015 in. Core depth . . . . 0.992 in. Density . . . . 4.4 lb/ft^3	Aluminum 5052-H39	Cell size . . . . 3/32 in. hex. Wall thickness . . . . 0.00075 in. Core depth . . . . 0.496 in. Density . . . . 4.4 lb/ft^3	Aluminum 5052-H39	Same as above except cells filled with 80-percent phenolic microballoon and 20-percent resin mixture to yield density . . . . 13.5 lb/ft^3
Fasteners	Steel A-286	Shank diameter . . . . . . 0.250 in.	Steel A-286	Shank diameter . . . . . . 0.125 in.	Steel A-286	Shank diameter . . . . 0.125 in.
Edge z-stiffener	Aluminum 7075-T6 extrusion	Variable across length	Aluminum 7075-T6 extrusion	Scaled variable across length	Aluminum 7075-T6 formed	Scaled variable across length
Adhesive	Bloomingdale HT-424	0.010 in. in bondline	Bloomingdale HT-424	0.005 in. in bondline	Bloomingdale HT-424	0.010 in. (approx) in bondline
Bolt pattern		Nominal 2.0 in. between centers		Exact 1:2 scaling		Exact 1:2 scaling

z-bars.- The z-bar closeouts were formed from 7075-T6 aluminum flat stock and then chem-milled to the scaled thicknesses depending on their location and the full-scale dimensions in that location. The bolt pattern was drilled in the outer web of the z-bar after final fabrication of the panel was completed.

Adhesives.- All face-sheet—core bonding was accomplished by use of HT-424 adhesive sheet with heat curing. All doublers were bonded to the skin in a similar fashion. The face sheets were bonded to the core under a partial vacuum to minimize internal pressure-induced peel failures when the panels were tested in a vacuum environment. The first two sandwich panels used HT-424 sheet adhesive between the core and z-bar closeout. The remaining panels used HT-424 foaming paste for this bond.

Doublers.- The full-scale panel utilized doublers on both the inner and outer face sheets to reinforce skin and core splice areas, areas around cutouts, and in three of the edge areas. The model panels, which did not have skin and core splices, did have scaled doublers in the proper locations.

Cutouts.- None of the access doors were simulated on the model panels. The cutouts for passage of the shelf-panel bolts were duplicated to the proper scale as shown in the detail sketch in figure II-1. A cylindrical cup bonded through the core and outer skin serves as a receptacle for the panel-shelf bolt. Circular doublers were used to reinforce the area around each receptacle. Also the honeycomb core around each receptacle was densified with filler to strengthen the area further.

Service module radial beam cap.- Since the test fixture was a boilerplate representation of bay 4 shape and volume, it was necessary to simulate the radial beam cap in order to scale the panel-beam interface strength. The simulation is illustrated in the detail sketch in figure II-1. A flat bar, having the proper thickness, bolt pattern, bolt hole diameter, and material properties was attached to the boilerplate radial beam by a clamping bar along each edge. Both the spacer plate and clamping bar were scored to prevent slippage in the clamped joint. The test panel was fastened to this simulated cap by scaled nut plates riveted to the inner surface of the cap.

Fasteners.- Geometric and material scaling required that the edge and shelf-panel fasteners be high strength A-286 steel screws with a shank diameter of 0.125 inch. The nearest size commercially available fastener in this material was a number 6 screw with a nominal shank diameter of 0.137 inch. Since one of the potential failure modes involved the shearing failure of these fasteners, number 6 screws were individually machined to the true scaled shank diameter of 0.125 inch. New fasteners were used for each test.

Panel mass.- The model sandwich panels weighed 13.3 pounds which corresponds to 106.4 pounds full scale. The actual weight of a full-scale panel is 98.8 pounds. When

the higher density honeycomb and filler in the model are considered, as well as a face-
sheet—core bond thickness which is double that desired, model weight within 8 percent is
considered to be within engineering tolerances.

III. APPARATUS AND INSTRUMENTATION

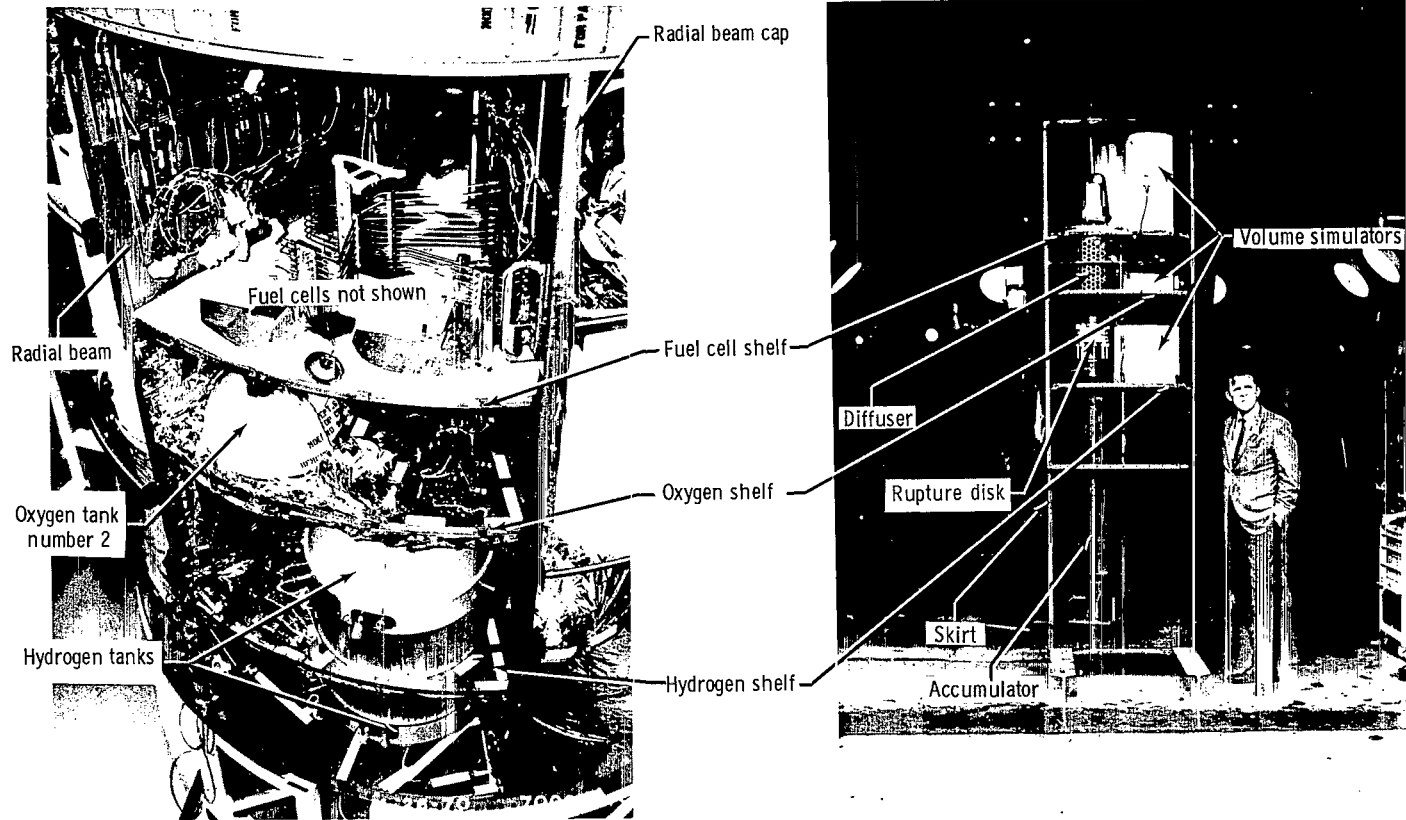By William R. Cofer, Derrill B. Chambliss, and James A. Osborn
Langley Research Center

Test Fixture and Pressurization System

The full-scale Apollo service module (SM) bay 4 is shown in figure III-1(a). This bay consists of a segment of the cylindrical service module between two radial beams or walls. The segment spans approximately 50°. A 44-inch-diameter tunnel on the service module center line is partially vented to bay 4 and the other 5 bays in the module. Shelves are located in bay 4 which serve as supports for three fuel cells, two cryogenic oxygen tanks, and two cryogenic hydrogen tanks. A curved cover panel is bolted to the outside of the bay, and forms part of the cylindrical service module exterior.

Since the bay 4 cover panel was completely removed from the flight vehicle at the time of the anomaly, and since one of the purposes of the present study was to investigate the pressure forces which could remove that panel, a boilerplate test fixture was constructed which would serve as the pressurization volume as well as a support structure for the test panels and the pressurization apparatus.

The test fixture is shown in figure III-1(b) with the pressurization system installed. The fixture consists of a one-half-scale geometric duplication of the basic bay 4 internal volume. No attempt was made to scale either mass, stiffness, or material properties of the full-scale internal structural members. All radial beams, shelves, and end closure plates were of 1-inch-thick steel. The nominal diameter of the tunnel was scaled but construction was of 1/2-inch-thick boilerplate. The remaining service module volume was simulated by a second boilerplate cylinder encompassing and tangent to the cylindrical tunnel. Vent areas between spaces inside bay 4, between these spaces and the tunnel, between the tunnel and the service module volume simulator, and between the tunnel and free space were modified during the test program to reflect both parameter study changes and increased knowledge of the full-scale vent areas and locations. The vent areas for each test are tabulated in the section "Discussion of Results." Some of the major bay 4 internal components were simulated on a volume basis as shown in figure III-1(b) to provide approximate internal volume and flow patterns. In the latter stages of the program, wooden mockups of the two cryogenic helium bottles in the upper part of the tunnel were also installed.

The pressurization system, also partially shown in figure III-1(b), consisted of a 10-gallon accumulator with the bladder removed and modified for remote filling, venting, and pressure monitoring. The pressurization gas was air and was supplied from a portable air compressor through two storage tanks. Pressure release was accomplished by

Radial beam cap

Fuel cells not shown

Radial beam

Fuel cell shelf

Oxygen shelf

Oxygen tank
number 2

Hydrogen tanks

Hydrogen shelf

Volume simulators

Diffuser

Rupture disk

Skirt

Accumulator

L-70-4775

(a) Full-scale bay 4.

(b) Half-scale test fixture in atmospheric
test facility.

Figure III-1.- Full-Scale Apollo service module bay 4 and half-scale model test fixture.

commanded mechanical puncture and subsequent failure of a standard commercial rupture disk rated just above the desired accumulator pressure. Gas flow from the accumulator was directed into the bay 4 space through a diffuser consisting of a cylinder (as indicated in fig. III-1(b)) with drilled vent holes through the cylinder wall. Since the oxygen tank number 2 (see fig. III-1(a)) was considered the most likely source of the anomalous flight pressurization, the diffuser was located so that its center line corresponded to the location of the oxygen tank center line. In some of the tests, the 90° segment of the diffuser nearest the test panel was blocked to reduce direct impingement effects on the panel. The diffuser could be placed to vent into the O_2 shelf space only or into both the O_2 and H_2 shelf spaces. One test was conducted wherein the diffuser was removed and the gas was directed vertically on to a plate on the lower surface of the fuel cell shelf.

As a guide to the test program, the pressure analysis of appendix B was utilized to predict bay 4 pressure magnitudes and distributions for proposed input and venting configurations.

<center>Test Facilities</center>

Atmospheric testing was conducted in a rocket test cell with the panel side of the test fixture near and directed toward the open side of the bunker. Vacuum tests were conducted in a 60-foot-diameter vacuum sphere at a nominal ambient pressure of 1.0 torr. In both instances, the test operational sequences were controlled by an automatic programed fire control circuit. This circuit was utilized to start and stop recorders and cameras and to initiate pressurization. Atmospheric tests were conducted with the test fixture bolted to a backstop. In the vacuum tests, the fixture was suspended from the top of the vacuum sphere by three cables. In this case, the fixture was loosely snubbed to cleats on the wall of the sphere to restrict reaction swinging motions.
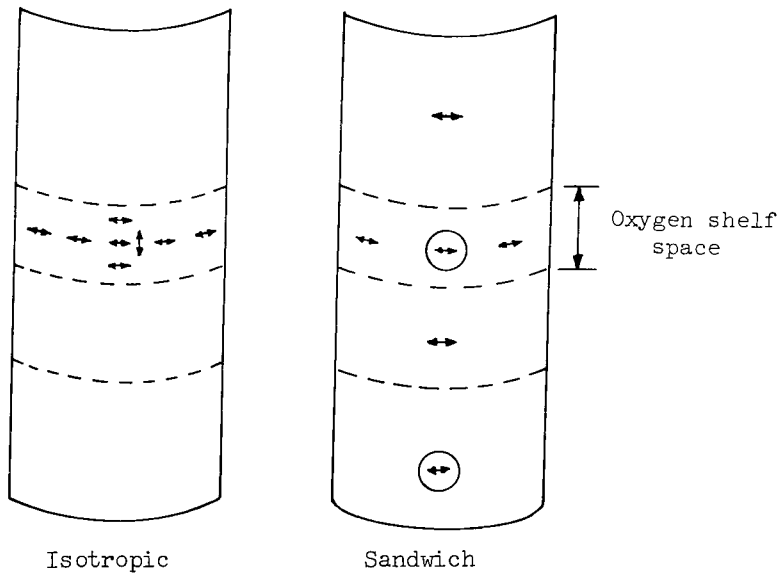
<center>Instrumentation</center>

The instrumentation recorded three different types of data: pressure gages measured pressure distributions within the test fixture; strain gages measured panel strains; and high-speed motion-picture cameras recorded panel failure modes and postfailure behavior.

Pressure data.- Inductance-type differential pressure transducers with a rating of 60 psid and a response time of less than 1/2 millisecond were installed in the test fixture in the pattern shown in figure III-2(a). Gages were placed in various locations in the oxygen shelf space and single gages monitored the pressures in each of the other compartments of the bay, the tunnel, and the service module volume simulator. Signals from these gages were conditioned through a 3-kilocycle carrier amplifier system and recorded as oscillograms for subsequent reduction. A 3000-psi strain-gage pressure transducer
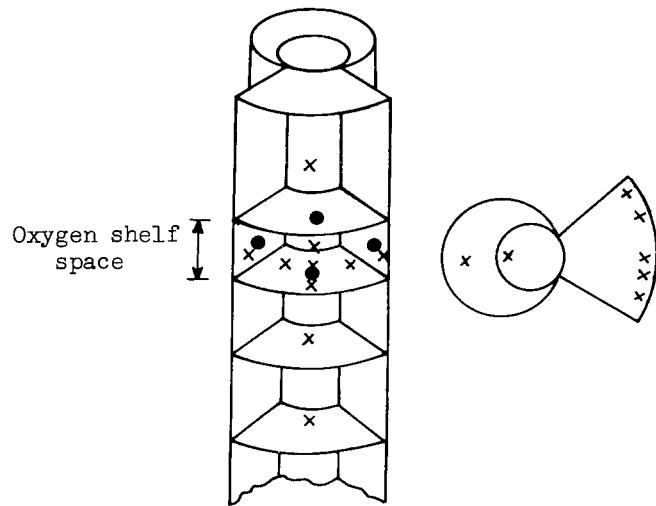
× Pressure gage near panel inner face
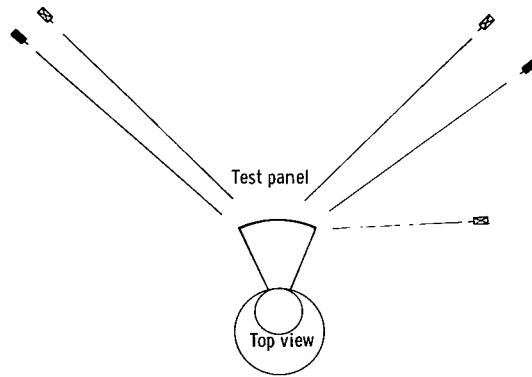
● Pressure gage in shelf or radial beam

(a) Pressure-gage locations.

Isotropic   Sandwich
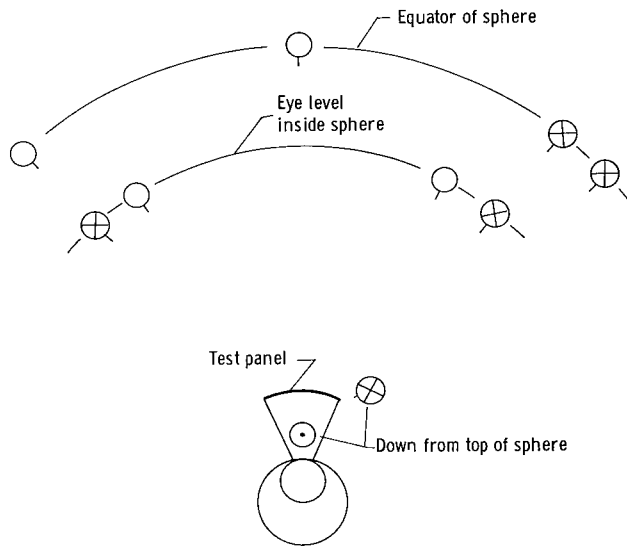
↔ External surface

(↔) External and internal surface

(b) Strain-gage locations.

Figure III-2.- Schematic of instrumentation.

Test panel

Top view

☞ Milliken 400 pps
■ Fastax 1000 pps

(c) Camera locations, atmospheric tests.

Equator of sphere

Eye level
inside sphere

Test panel

Down from top of sphere

⊗ Milliken 400 pps
◯ Fairchild 2000 pps

(d) Camera locations, vacuum tests.

Figure III-2.- Concluded.

along with the carrier amplifier conditioning equipment was used to monitor and record the accumulator pressure. In addition, a dial-type pressure gage was installed in the accumulator fill line near the remote air supply system.

Strain data.- The isotropic and sandwich panel models were instrumented with strain gages as shown in figure III-2(b). The gages were of the single-arm-bridge type with the dummy bridge arms in a box affixed to the side of the test fixture. Gage outputs were passed through the 3-kilocycle carrier amplifier system and recorded as oscillograms. The strain data were utilized only for evaluation of panel behavior and in planning of subsequent tests and are not presented in this paper.

Photographic data.- High-speed motion-picture cameras were used to examine the failure modes and postfailure behavior of the panels. Different camera types and locations were used in the atmospheric and vacuum tests. The camera locations, camera speeds, and types for the two test setups are shown in figures III-2(c) and III-2(d). As an aid in interpreting the photographic data, a grid of 1/4-inch lines approximately 6.9 inches between centers was painted on the test panels.

IV. STRUCTURAL ANALYSIS OF APOLLO 13 BAY 4 COVER PANEL

By Martin M. Mikulas, Jr., and Deene J. Weidman
Langley Research Center

The analytical investigation conducted in parallel with the experimental investigation is summarized in this chapter. The analytical effort can be categorized as follows:

(1) Nonlinear transient response of the panel to rapid pressure loadings

(2) Panel edge load distribution produced by various static-pressure distributions

(3) Effect of cutouts on failure load

(4) Effect of puncture on failure load.

The first analysis used a special-purpose computer program for transient analysis of nonlinear structures. The last two analyses utilized NASTRAN (NASA Structural Analysis). Results from the transient analysis program indicated that for pressure rise times that could have occurred during the Apollo 13 incident, the structural behavior of the bay 4 panel was essentially static in nature. For this reason, most of the calculations made on the panels were conducted by use of a static nonlinear NASTRAN analysis. Although the bay 4 panel suffered plastic deformations before failure occurred, the plastic option available in NASTRAN was not exercised because of the time constraint.

Structural Idealization

The idealized configuration which was used in both computer programs is shown in figure IV-1 for both the isotropic and sandwich model panels. For both panels, the sheet material was aluminum and the properties are listed. In addition, for the sandwich panel, the density of the core ρ_c is given.

The panel was assumed to be simply supported at its neutral surface around the edges. In addition, no account was taken of the widely spaced shelf bolts which attach to the central portion of the panel, since they would simply pull through when the panel was internally pressurized without affecting the overall behavior of the panel.

Transient Analysis

An analysis of the transient response of the bay 4 panel subjected to various pressure distributions and various pressure rise times was conducted to determine the importance of dynamics in panel separation. The analysis was conducted on a new University of Virginia computer program which was developed under NASA grant number NGL-47-005-098 to study dynamic buckling of doubly curved shells. This computer
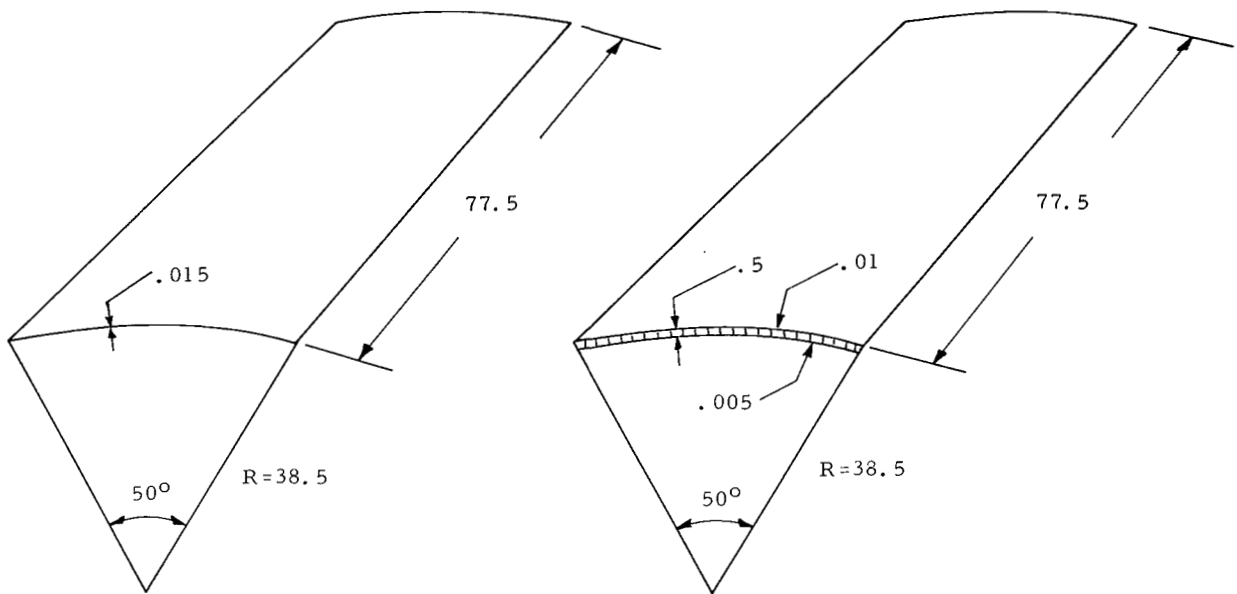
(a) Isotropic panel. $E = 10.4 \times 10^6$ psi; $\nu = 0.3$; $\rho_S = 0.1$ lb/in^3.

(b) Sandwich panel. $E = 10.4 \times 10^6$ psi; $\nu = 0.3$; $\rho_S = 0.1$ lb/in^3; $\rho_c = 3.1$ lb/ft^3.

Figure IV-1.- Half-scale isotropic and half-scale sandwich panel configurations used in computer programs. All linear dimensions are in inches.

program, designated TAONS, is a finite-difference formulation of the nonlinear shallow shell equations with time dependency incorporated by using the beta method.

Discussion of Analysis

In order to obtain a clean separation of the bay 4 panel, the initial failure was believed to have occurred along an edge of the panel and progressed in an unzipping fashion. For this reason, the edge loads on the panel were the focal point of the analytical investigation. It was determined very early that for various pressure loadings, edge loads on the upper and lower ends of the panel were not significant and that the initial failure would have to occur along a vertical edge of the panel because of excessive hoop stresses. Further evidence that the initial failure would occur along an edge was provided by pull tests of narrow tensile specimens which modeled the membrane properties of the half-scale panels. These tests indicated that a shear tear out of the panel around the bolts would be the expected failure mode. Results of these pull tests are presented in appendix A. The balanced design of the panel, wherein the membrane strength and bolt shear strength are nearly equal along the vertical edge, also supported the decision to study the edge loads analytically.

The transient analysis program was exercised on both the half-scale isotropic and the half-scale sandwich panels. In order to obtain reasonable results for stresses in the panel, both the time increments and station spacing had to be chosen relatively small and, as a result, computer running time became very long. Most of the calculations were performed for the isotropic half-scale panel. Checks were made on the half-scale sandwich panel to assure that a correspondence existed.

The types of pressure time histories that were used in this investigation are shown in sketch IV(a). Essentially, the pressure was assumed to increase in a linear fashion to
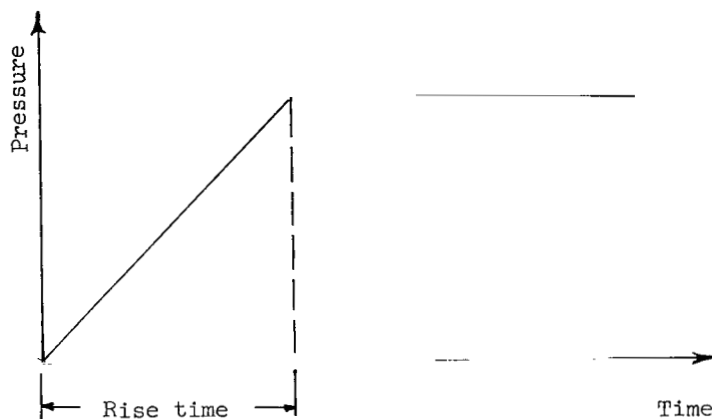
Sketch IV(a).- Pressure time history used in transient analysis.

a maximum value and then remain constant. In figure IV-2, the maximum edge load N_{max}, nondimensionalized with respect to pR, has been plotted for the half-scale isotropic panel as a function of time for various values of the rise time. The results in figure IV-2 are for a uniform pressure over the whole panel. For the case where the rise time is zero (a step pressure loading), figure IV-2 shows that the effect of dynamics is very significant, edge loads approximately twice the linear static value of pR being obtained. For rise times of 0.001 second and greater, the effects of dynamics are greatly reduced. A case was also run where the pressure was applied over the O_2 shelf area only. Although the maximum edge load decreased somewhat because of diffusion into the panel, conclusions as to the relative importance of dynamics were the same as those for the previous case. Check cases on the half-scale sandwich panel indicated that the effect of the added bending stiffness of the sandwich changed the maximum edge loads by less than 5 percent. The results shown in figure IV-2 are also applicable to the full-scale bay 4 panel if the time scale is doubled.

These results indicated that for pressure rise times greater than 0.001 second (0.002 second for full scale), the effects of dynamics on the maximum panel edge load
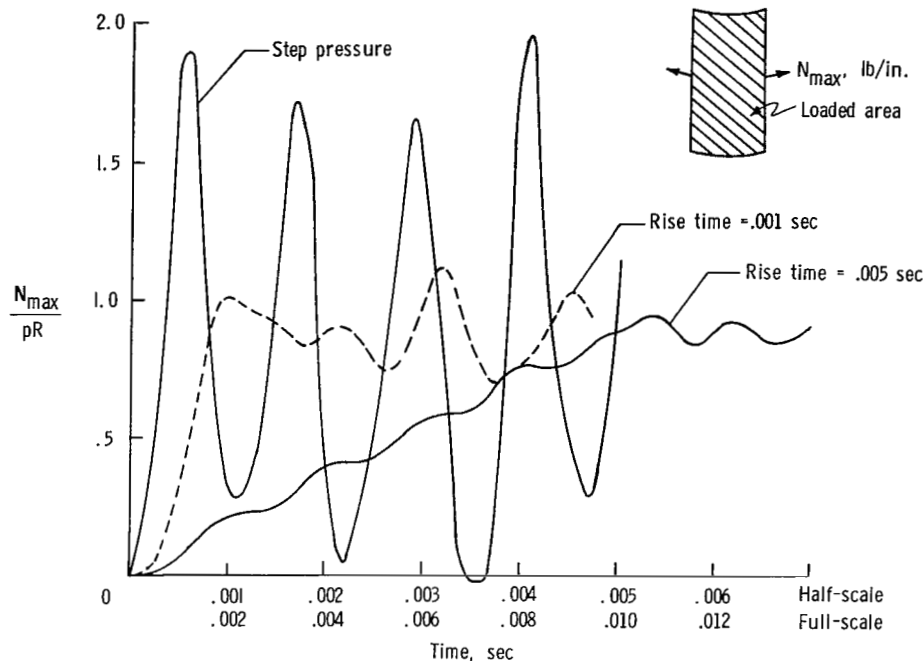
Figure IV-2.- The effects of pressure rise times on the dynamic
response of the Apollo 13 bay 4 panel.

are very small. Thus, most of the calculations for determining maximum edge loads on the panels were performed on the more seasoned NASTRAN computer program by use of a static analysis.

Panel Edge Loads

In this section some of the results of an investigation which was conducted to determine the effects of pressure distribution on the panel edge loads and peak values of pressure required for panel failure are presented. The results were obtained from a static elastic NASTRAN analysis. Because of the predominant membrane behavior of the panel, however, it was necessary to exercise the nonlinear option offered in NASTRAN to obtain meaningful answers. For all cases considered, the panel was divided into 16 elements along the length and 12 elements across the width. Because of symmetry across the panel, however, only one-half of the panel was considered.

In figure IV-3, the maximum edge load as a function of pressure is presented for the half-scale sandwich panel for three different static-pressure distributions. The three pressure distributions considered were: a uniform pressure over the whole panel, twice as much pressure on the O_2 shelf area as on the rest of the panel, and pressure on the O_2 shelf area only. Also shown for comparison purposes is the linear membrane result, $N_{max} = pR$. The lower sketch on the right-hand side of figure IV-3 shows where the
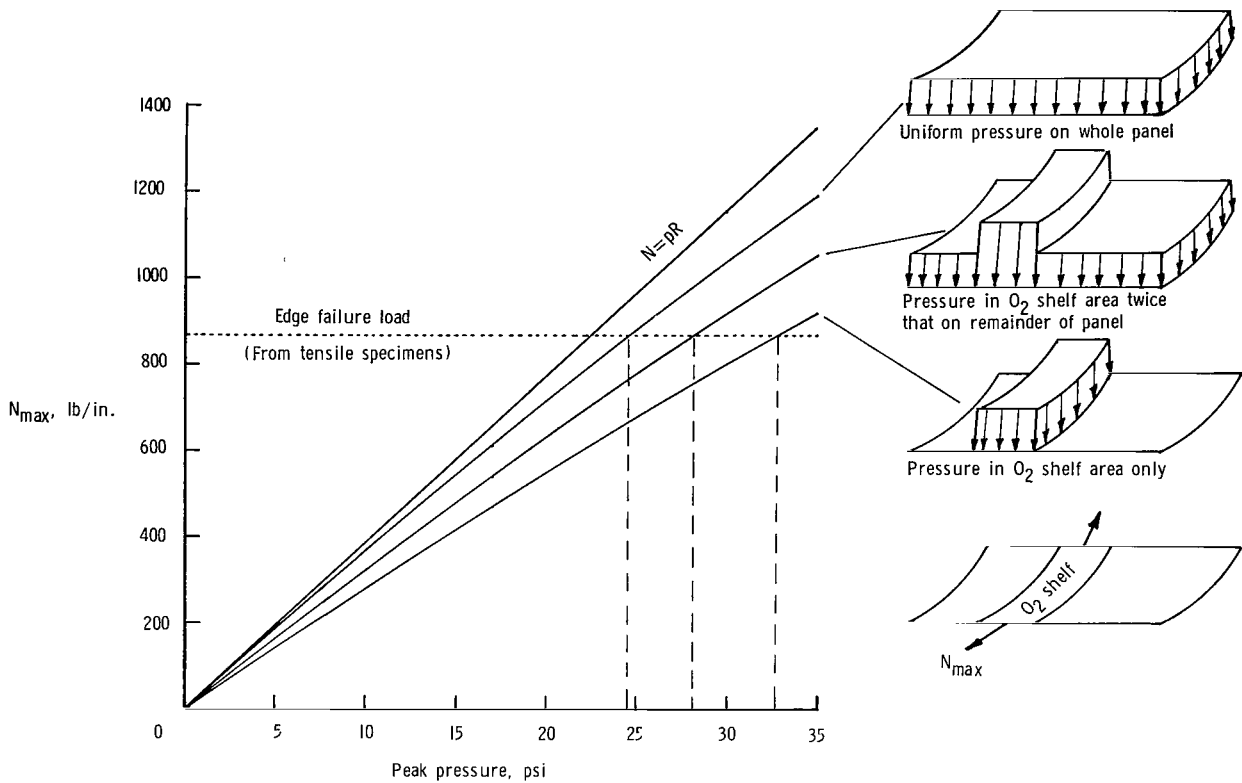
Figure IV-3.- Peak pressures required to fail panel for different pressure distributions.

maximum edge load occurred for the two nonuniform loadings whereas for the uniform pressure loading the hoop edge load was essentially constant over the length of the panel. The horizontal dotted line indicates the value of edge failure load to be expected on the half-scale panels. This value was determined as described in appendix A from pull tests and tensile shock loading tests on 2-inch-wide tensile specimens of the isotropic half-scale panels. It can be seen in figure IV-3 that for the different cases considered the value of pressure required to initiate an edge failure is ≈33 psi if the O_2 shelf area is the only area pressurized, ≈29 psi if half the peak pressure is added to the remainder of the panel, and ≈24 psi if the whole panel is pressurized uniformly. Results from the analysis indicate that the peak pressure required to fail the isotropic panels is about 5 percent less than that required to fail the sandwich panels. As was shown in "Dynamic Models," the scaling for the half-scale models was such that the failure pressures reported herein are the same values as would be required to fail the full-scale panel.

Additional insight as to the nature of the pressure distribution required to separate the whole panel from its supports can be obtained from the edge load distributions and their directions for various pressure distributions. In figure IV-4 the edge load vectors are shown for two different pressure distributions. Since the loading is symmetric,
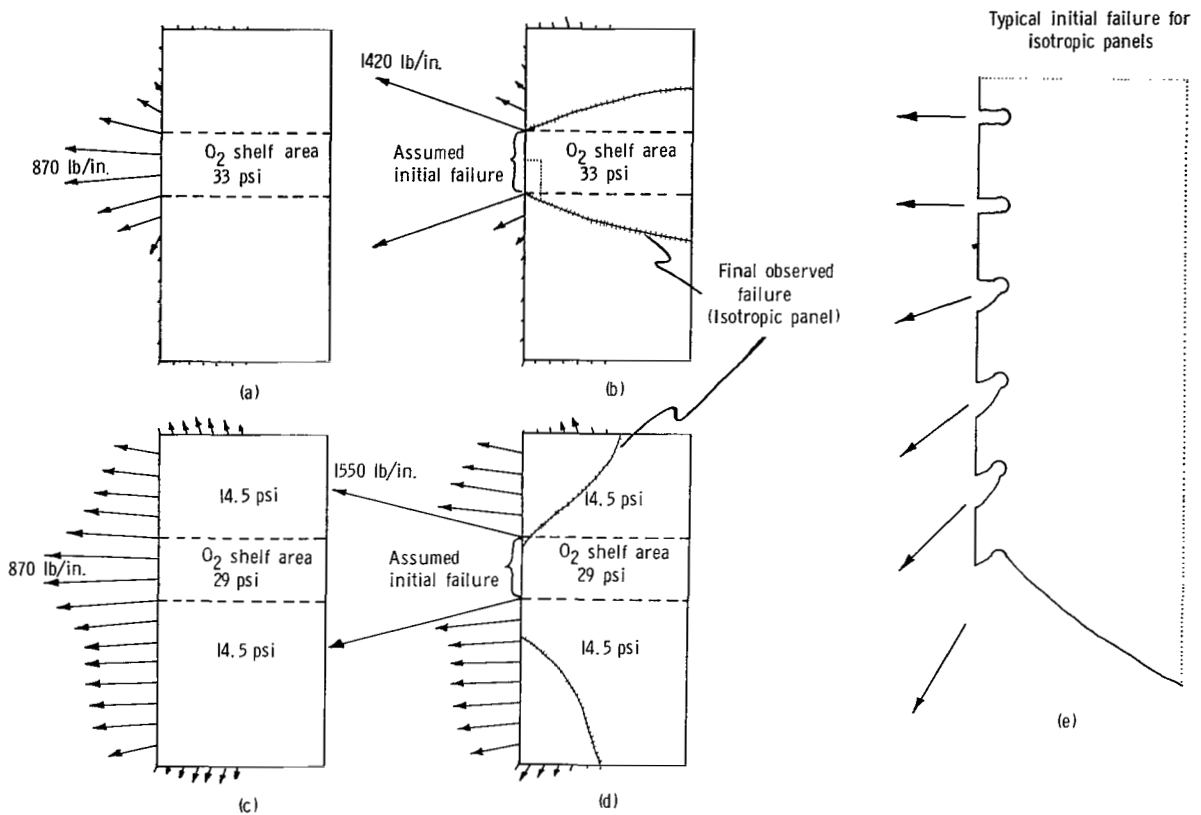
Figure IV-4.- Distribution of edge loads on half-scale Apollo 13 sandwich
panel as predicted by NASTRAN.

only the load vectors on one side of the panel are shown. In figure IV-4(a), the edge load vectors are shown for the case where only the O_2 shelf area is pressurized. The load drops off very rapidly away from the O_2 shelf and the direction of loading does not remain normal to the panel edge. In figure IV-4(b), the edge load distribution is shown for the same pressure loading case where part of the edge is assumed to have already failed. A large load concentration results at the ends of the failed region; however, the rotation of the load vectors away from perpendicular to the panel edge tend to force the failure into the center of the panel. This phenomenon was observed in the tests on the isotropic panels where only the O_2 shelf area was pressurized and a typical observed failure is shown in figure IV-4(b). Under such loadings only local areas of the panel were removed. The sketch in figure IV-4(e) is a blown up section of the initial failure region of figure IV-4(b) and shows the observed shear type tear outs around the bolts. The initial tear outs in the middle of the O_2 shelf region were normal to the panel edge and subsequent tear outs were rotated in the directions as indicated by the arrows until one side of the tear out eventually propagated into the center of the panel. The direction of the

observed tear outs has the same trends as would be expected from the load vectors predicted by the analysis.

In figure IV-4(c) the edge load vectors are shown for the case where half the peak pressure is applied to the remainder of the panel. It can be seen that the load vectors are much more uniform and remain nearly normal to the panel edge. In figure IV-4(d), the edge load vectors are shown for the same pressure case where part of the edge has already failed. As in the case where only the O_2 shelf area was pressurized, a very large load concentration exists at the edge of the failed region. However, the edge load directions remain nearly normal to the edge and could thus cause the crack to run up and down the panel rather than across as in the previous case. In figure IV-4(d), a typical observed failure for an isotropic panel with approximately this type of pressure loading is shown. For the case where the pressure is applied uniformly over the whole panel, the edge load distribution is very uniform and perpendicular to the panel edge except in a very small region at the panel corners. The edge loads for this case are not shown here; however, a test on an isotropic panel which was nearly uniformly loaded did verify that the failure will propagate along the entire edge and leave only very small triangular tabs in the corners.
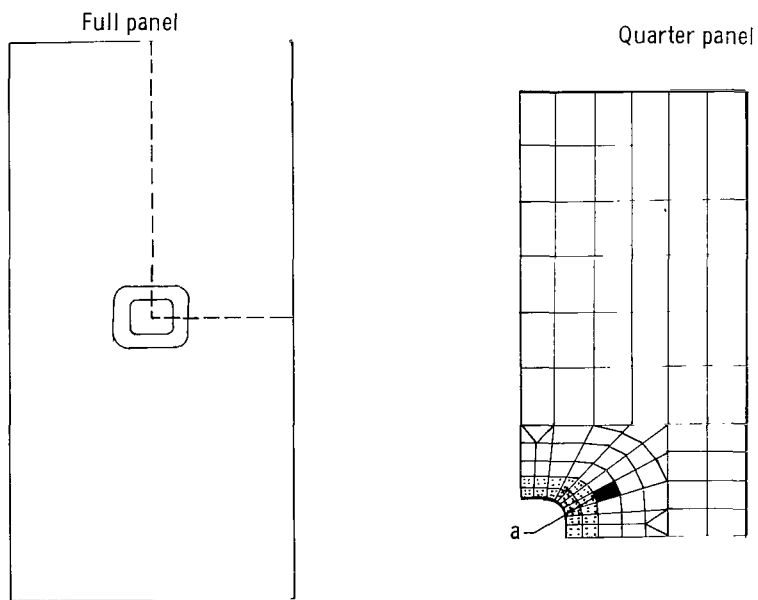
Effect of Cutouts on Failure Pressure

The question arose as to whether the cutouts which existed on the Apollo 13 bay 4 panel could have provided a mechanism for significantly lowering the pressure required for complete failure of the panel. To gain insight into this question, a model of one of the cutouts was analyzed with the NASTRAN computer program to determine whether changes in stress could be expected around the cutout. A sketch of the full-scale bay 4 panel showing 8 cutouts is shown on the left of figure IV-5(a). All cutouts are reinforced with doublers and have cover plates bolted on. The cutout chosen for investigation is labeled A, and a blowup showing its dimensions is shown in the upper right of figure IV-5(a). The configuration which was actually analyzed is shown on the left-hand side of figure IV-5(b). In this analysis configuration, cutout A of figure IV-5(a) has been shifted to a central location on the panel to establish a symmetric idealization and this shift results in a considerable saving of computer running time.

The finite element modeling used in NASTRAN is shown on the right-hand side of figure IV-5(b). Only a quarter panel was analyzed because of the symmetry involved. The dotted elements represent the reinforced area around the cutout. Results of the analysis indicate that the cutout does not cause large increases in stress. In fact, the largest increase was 10 percent in the principal stress which occurred in the element labeled a in figure IV-5(b). Such an increase would lower the present failure level of pressure (approximately 30 psi) to no less than 27 psi. Thus, cutouts in the Apollo 13 panel do not provide a mechanism for substantially lowering the pressure required for failure.
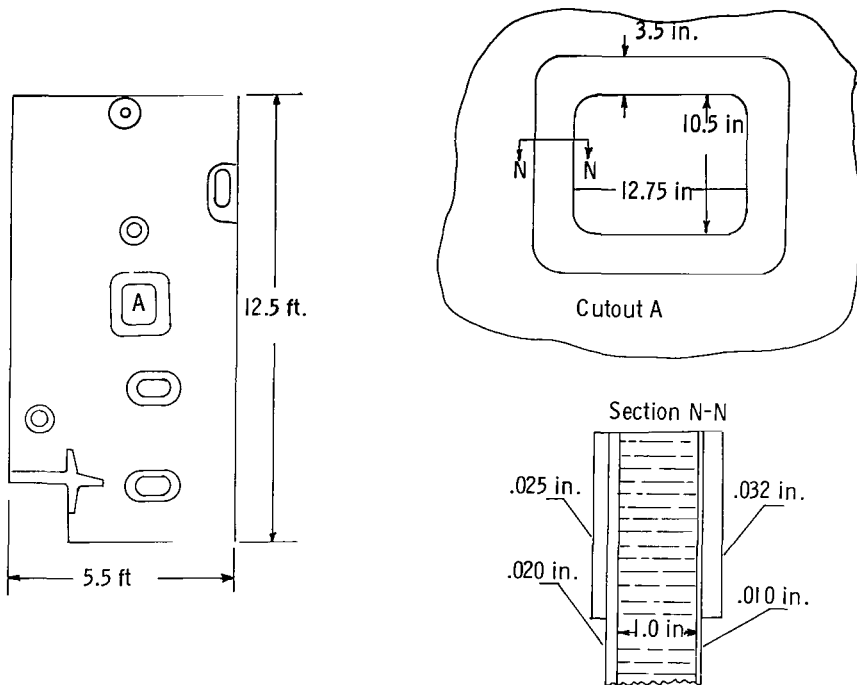
(a) Full-scale cutouts.

(b) NASTRAN idealization.

Figure IV-5.- Full-scale panel with cutouts and NASTRAN
idealization of panel with single cutout.

Effect of Panel Damage on Failure Pressure

Another possibility for substantially lowering the pressure required to fail the bay 4 panel is for the panel to be weakened by damage from a flying particle. For instance, if a particle penetrated the panel and caused a sharp-edged hole, a very large stress concentration would result and would thus provide a mechanism for complete failure of the panel at much reduced pressures.

To determine the size hole needed to reduce the failure pressure of the full-scale Apollo 13 bay 4 panel to a prescribed level, a fracture mechanics analysis was conducted. The results are shown in figure IV-6. The ratio of the pressure required to propagate an initial rip or sharp-edged hole divided by the pressure required to fail an undamaged panel is plotted as a function of the damage size. The results of two different fracture approaches are included in the figure. Although there are some differences in the results of the two approaches, both indicate that about a 5-inch-long hole or rip would lower the pressure required to fail the panel completely to one-half of the value of pressure required to fail an undamaged panel. As indicated by the figure, a larger initial rip would result in even lower failure pressures.
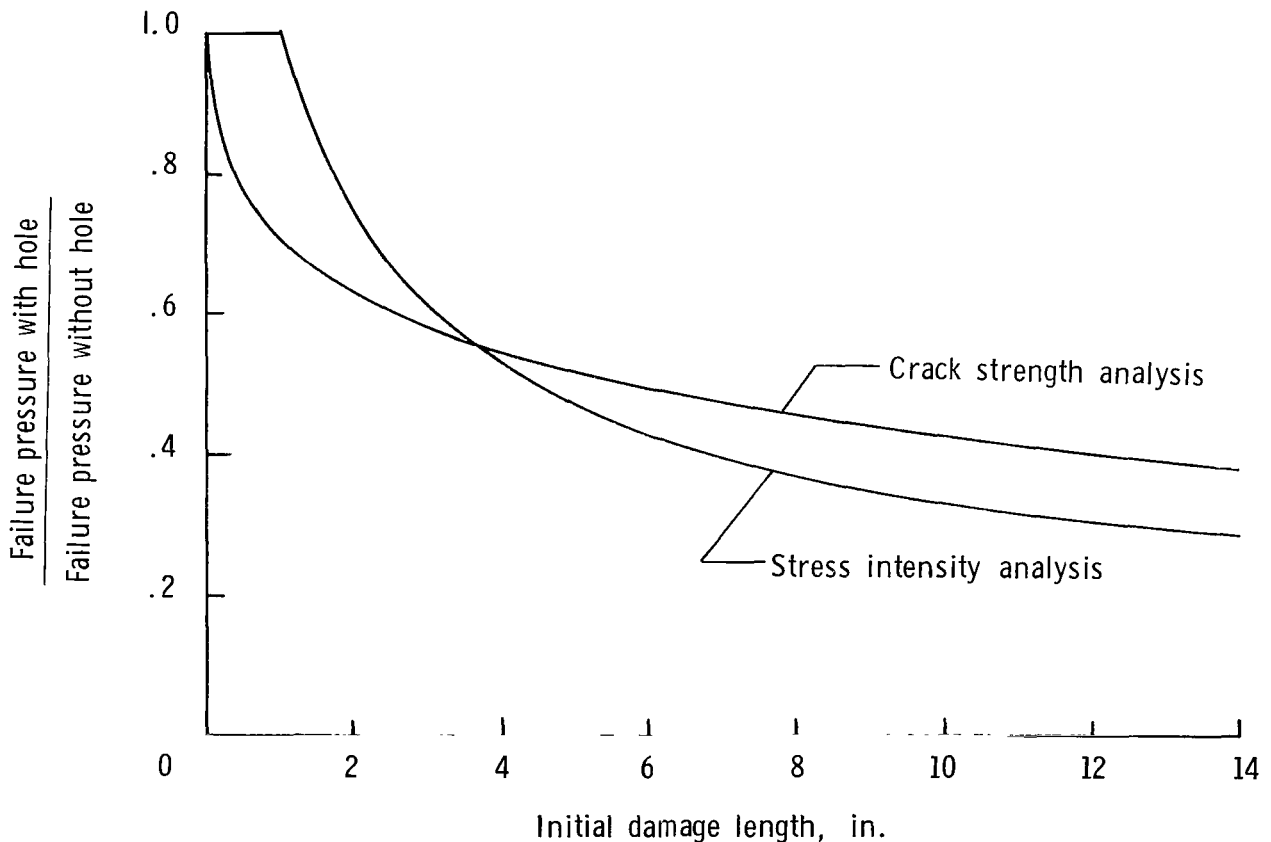
Figure IV-6.- Effect of initial damage on full-scale panel failure pressure.

Analytical Results

The principal results of this analytical investigation may be summarized as follows:

1. For pressure rise times that can be rationalized to have occurred during the Apollo 13 incident, shell dynamics were found to play an insignificant role in the panel failure.

2. The peak pressure required to fail the bay 4 panel could vary from 24 psi to 33 psi depending upon the type of pressure distribution applied.

3. For locally pressurized panels, the rapid dropoff of edge load with an accompanying change in direction of the load vector away from normal to the edge suggests that a failure can be expected to propagate into the panel rather than along the edge. Attainment of significant edge loads over the full length of the panel such as would be required for complete separation, requires substantial pressure loading over most of the panel.

4. The presence of cutouts in the bay 4 cover panel does not substantially affect the magnitude of the failure pressure.

5. The presence of a sharp-edge tear or penetration in the panel can substantially lower the pressure required for complete failure.

Although direct comparison between theory and experiment for the pressurized panels has not been attempted, a qualitative comparison indicates that the theory does support the experimental conclusions in "Discussion of Results" relative to the level of pressure required to fail the panel and the type of pressure distribution required for a clean separation.

V. DISCUSSION OF RESULTS

By Homer G. Morgan, H. Wayne Leonard,
and William R. Cofer
Langley Research Center

Presentation of Results

The test program and its results are summarized in table V-I. Three series of tests made up the total program: (1) atmospheric tests using isotropic panels, (2) vacuum tests on isotropic panels, and (3) vacuum tests with sandwich panels. Two general types of panel separations were observed: localized failures when part of the panel near the pressure source separated, and failures wherein the complete panel separated from the test fixture. Even in those cases with no separation, structural damage due to shelf bolt head pullthrough occurred.

Table V-I also indicates the range of peak pressures measured in the oxygen shelf space during each test. The complex transient flow pattern existing within the space during rapid pressurization is believed to account for the spread in these pressure values. Pressure rise times, measured from pressure release to peak pressure or to failure, depended on the source pressure, input flow rate, and internal venting of the test fixture. Table V-II, defines the pressurization input parameters, the internal venting, and internal volumes for each test.

Typical pressure time histories measured during the three test series are shown in figures V-1, V-3, and V-5. Figures V-2, V-4, and V-6 present sequences from high-speed motion-picture cameras illustrating the types of separations that occurred. Photographs in figure V-7 show details of edge failures on both isotropic and sandwich panels.

Atmospheric Tests With Isotropic Panels

The initial series of five tests on isotropic panel models was conducted under atmospheric pressure conditions. Panel separations of the type sought were not completely achieved. However, with panels DM-3 and DM-4, nearly total separations were achieved by very rapid but relatively uniform pressurization of the entire bay 4 volume as shown in figures V-1(b) and V-1(c). The photographic sequences presented in figure V-2(a) indicate that initial failure of panel DM-3 was by edge separation near the pressure source. Diagonal tears through the panel then permitted doorlike opening of the fragments by the internal pressure forces. Figure V-2(b) shows that failure of panel DM-4 started with a crack where a shelf bolt pulled through the panel. The failure propagated as a pair of vertical tears on opposite sides of the panel and the center section of the panel was blown free of the test fixture.

TABLE V-I

SUMMARY OF PANEL SEPARATION TESTS

Model	Discharge location	Diffuser configuration	Pressure [1]		Separation
			p, psi	Rise time, sec	
		Atmosphere tests with isotropic panels			
DM-1-1	O_2 shelf	Open	24 to 30	0.020	None
DM-1-2	O_2 shelf	Open	30 to 58	.005	O_2 shelf area
DM-2	O_2 shelf	Open	34 to 52	.006	O_2 shelf area
DM-3	O_2 and H_2 shelves	Open	15 to 35	.015	Nearly total (folded back)
DM-4	O_2 and H_2 shelves	Shielded	20 to 44	.016	Nearly total (left edges)
		Vacuum tests with isotropic panels			
DM-5-1	O_2 and H_2 shelves	Shielded	14 to 20	----	None
DM-5-2	O_2 and H_2 shelves	Shielded	20 to 28	0.016	Total
DM-6	O_2 and H_2 shelves	Shielded	19 to 27	.018	Total
DM-7	O_2 shelf	Open	25 to 40	.005	O_2 shelf area
DM-8	O_2 shelf	Shielded	20 to 37	.012	O_2 shelf area
DM-9	O_2 shelf	Shielded	18 to 23	.040	None
DM-10	O_2 shelf	Shielded	21 to 39	.070	Upper two-thirds of panel
		Vacuum tests with sandwich panels			
HS-1	O_2 shelf	Shielded	-------	----	None
HS-2	O_2 shelf	Shielded	23 to 47	0.190	Total
HS-3	O_2 shelf	Shielded	31 to 67	.020	Total
HS-4	O_2 shelf	Shielded	30 to 44	.020	None
HS-5	O_2 shelf	None	23 to 52	.012	Upper two-thirds of panel

[1] Range of peak pressures in the O_2 shelf space is indicated. Time from pressure release to peak pressure or to failure is rise time.

TABLE V-II

SUMMARY OF PRESSURIZATION SYSTEM PARAMETERS
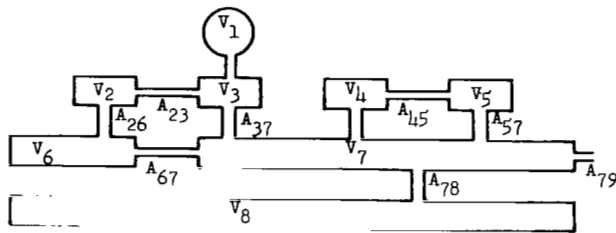
Volume	Description
1	Pressurization tank
2	Fuel cell space
3	O_2 tank space
4	Upper H_2 tank space
5	Lower H_2 tank space
6	Upper tunnel
7	Lower tunnel
8	Other SM free volume

Model	Pressure source[a] A_{13}, in²	p_o, psig	— Free volume, in³							Vent area, in²								
			V_2	V_3	V_4	V_5	V_6[c]	V_7[c]	V_8	A_{23}	A_{26}[b]	A_{37}[b]	A_{45}	A_{47}	A_{57}	A_{67}	A_{78}	A_{79}
Atmosphere tests with isotropic panels																		
DM-1-1	2.86	1375	9440	4220	8620	8970	39 200		127 500	0	81	37	100	81	81	365	1680	7.5
DM-1-2	2.86	3100	9440	4220	8620	8970	39 200		127 500	0	81	37	100	81	81	365	1680	7.5
DM-2	2.86	3000	9440	4220	8620	8970	39 200		127 500	0	81	37	100	81	81	365	1680	7.5
DM-3	2.86	3030	9440	4840	7740	9310	39 200		127 500	123	81	37	100	81	81	365	1680	7.5
DM-4	2.86	3030	9440	4840	7740	9310	39 200		127 500	123	81	37	100	81	81	365	1680	7.5
Vacuum tests with isotropic panels																		
DM-5-1	2.86	2000	9440	4840	7740	9310	39 200		127 500	123	81	37	100	81	81	365	1680	7.5
DM-5-2	2.86	3030	9440	4840	7740	9310	39 200		127 500	123	81	37	100	81	81	365	1680	7.5
DM-6	2.86	3035	9440	4840	7740	9310	39 200		127 500	123	81	37	100	81	81	365	1680	7.5
DM-7	2.86	3000	9440	4220	8620	8970	39 200		127 500	0	81	37	100	81	81	365	1680	7.5
DM-8	1.2	3000	9540	4220	8620	8970	39 200		127 500	0	81	37	100	81	81	365	1680	7.5
DM-9	.4	3000	9540	4220	8620	5700	39 200		127 500	0	81	37	100	81	81	365	1680	7.5
DM-10	.8	3000	8550	5600	8620	6950	3 460	26 800	127 500	27	136/50	80/51	100	160	136	24	20	15.6
Vacuum tests with sandwich panels																		
HS-1	0.8	3000	8550	5600	8620	6950	3 460	26 800	127 500	27	136/50	80/51	100	160	136	24	20	15.6
HS-2	1.2	3000	8550	5600	8620	6950	3 460	26 800	127 500	27	136/50	80/51	100	160	136	24	0	15.6
HS-3	2.86	3000	8550	5600	8620	6950	3 460	26 800	127 500	27	136/50	80/51	100	160	136	24	60	15.6
HS-4	2.0	3000	8550	5600	8620	6950	3 460	26 800	127 500	27	136/50	80/51	100	160	136	24	120	15.6
HS-5	2.86	3000	8550	5980	8620	6950	3 460	26 800	127 500	27	136/50	80/51	100	160	136	24	60	15.6

[a] $V_1 = 2260$ in³.

[b] Larger number of double entries is measured vent size between compartments. Smaller number is effective vent area due to constriction around simulated internal tanks.

[c] Larger number of double entries is volume in bottom of tunnel. Smaller number is volume in top of tunnel.
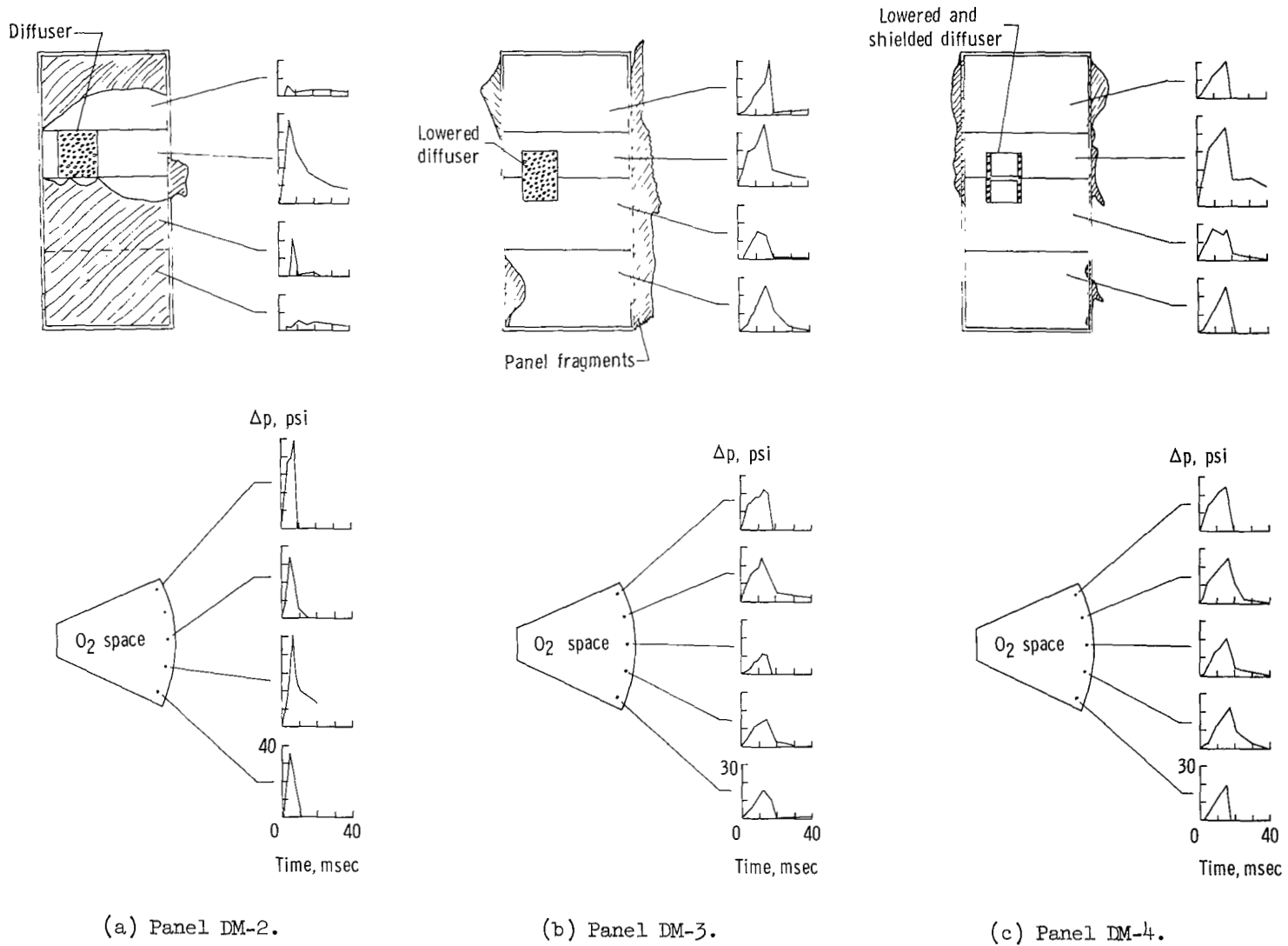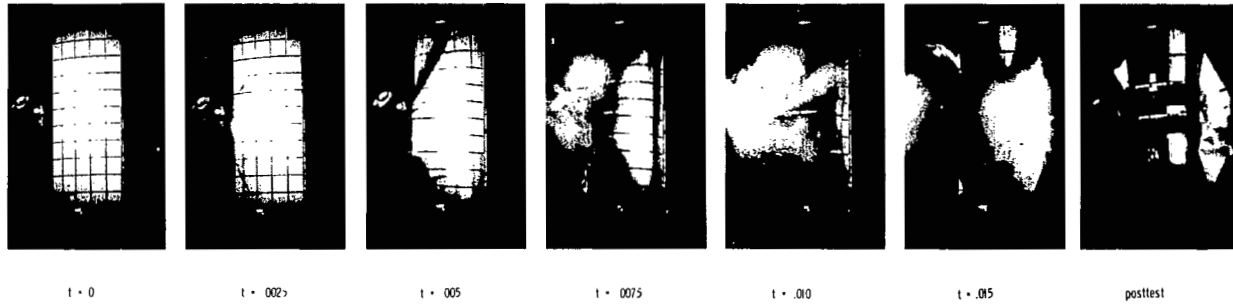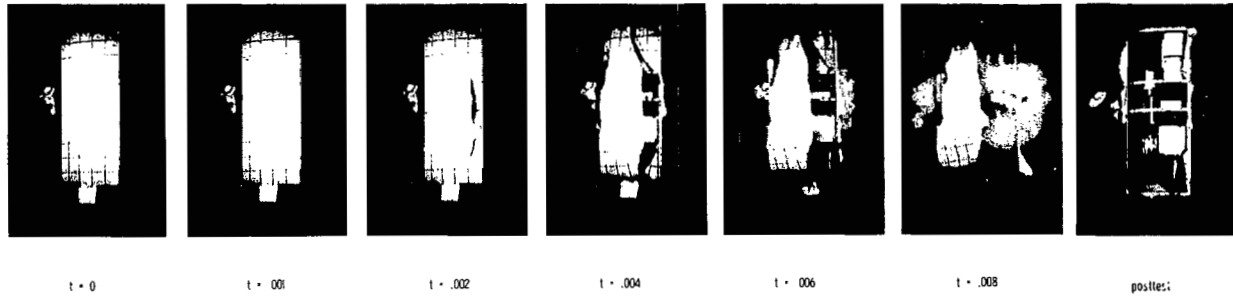
(a) Panel DM-2. (b) Panel DM-3. (c) Panel DM-4.

Figure V-1.- Pressure time histories of isotropic panels in atmosphere. (The time is from initial pressure release.)

t = 0   t = .002⁵   t = .005   t = .0075   t = .010   t = .015   posttest

(a) Panel DM-3.

t = 0   t = .001   t = .002   t = .004   t = .006   t = .008   posttest

L-70-4776

(b) Panel DM-4.

Figure V-2.- Sequential failure of isotropic panels in atmosphere. (t is the time
from first observed failure.)

Panel DM-2 was failed by highly localized pressure loadings in the oxygen shelf space as shown in figure V-1(a). Initial failure was separation of the panel edge over the oxygen shelf space. Circumferential tears across the face of the panel then allowed the entire area over the oxygen shelf space to open (doorlike). Inertia loads then separated a large fragment of the panel from the test fixture, but about two-thirds of the panel was left in place. This failure was typical of tests conducted with rapid localized pressurization in the oxygen shelf space.

The initial failure, as well as the direction of the postfailure tear for both types of failures, correlates with the NASTRAN calculations. Highly nonuniform loadings, of which the test on panel DM-2 is representative, result in nearly circumferential tears that leave large sections of the panel intact. More uniform loadings, represented by tests on panels DM-3 and DM-4, result in hoop-tension-type stresses that cause the tear to propagate longitudinally through the panel and result in more extensive damage.

The edge separations that occurred in this test series were typical of all tests on isotropic panel models and are illustrated in figure V-7(a). In general, the failure consisted of debonding between the face sheet and z-bar accompanied by face sheet tear-out around the bolts. The z-bar remained on the test fixture, and attachment bolts were left intact. Exceptions to this type of local failure occurred along the upper edge of the panel (that had a thinner gage z-bar) when both the skin and z-bar pulled through, apparently without debonding, but left the attachment bolts intact.

Vacuum Tests on Isotropic Panels

The second series of tests were conducted with isotropic panel models in a vacuum chamber at an ambient pressure of 1 torr. Five partial or total separations were achieved in seven tests. Typical pressurization histories are presented in figure V-3, and photographic sequences of the failures appear in figure V-4.

Behavior of isotropic panels in vacuum is much the same as isotropic panel behavior during atmospheric tests. Initial failure mechanisms (fig. V-4) and edge separations (fig. V-7) are identical to those in atmospheric tests. Tears propagate across the panels in similar fashion, as can be seen by comparing figures V-2 and V-4. Postfailure behavior is also similar although more violent in vacuum. Increased dynamic action after the initial failure is primarily due to the removal of the virtual air mass (about 25 percent of isotropic panel mass) and air damping. Without these retarding forces, expansion of gas from the test fixture accelerates panel fragments to very high velocities. Thus, inertia loads are much higher than those obtained during atmospheric tests. These inertia loads and changes in the complex gas flow due to lower ambient pressures are believed to cause the total separation in vacuum that could not be achieved in atmosphere.

Panel DM-7 (figs. V-3(b) and V-4(b)) was tested in vacuum with all other parameters identical to those during the atmospheric test on panel DM-2 (fig. V-1(a)). Although some details of the pressurization and behavior during failure varied slightly between tests, the final result was nearly identical local separations over the oxygen shelf space.

During this test series, a new internal flow configuration of the test fixture was introduced before testing panel DM-10. This configuration, which has been described in table V-II, resulted from improved information about the full-scale spacecraft and was believed to simulate the flight conditions more closely. An analysis that predicts pressures for this configuration is presented in appendix B. The new configuration permits pressure to increase more uniformly over the oxygen and fuel-cell shelf spaces, while pressure build-up in the hydrogen shelf spaces lags behind. The results from panel DM-10 (figs. V-3(c) and V-4(c)) illustrate that the effect of very rapid pressurization over the upper two shelf spaces is to separate the upper two-thirds of the panel while the lower one-third is left intact. The edge separation of panel DM-10 during failure was similar to that of other isotropic panels.

Vacuum Tests on Sandwich Panels

The final test series used honeycomb sandwich panels that were one-half-scale models of flight structure so that strength, membrane stiffness, and bending stiffness were appropriately scaled. The tests were conducted in vacuum at 1 torr ambient pressure and used the revised internal flow configuration of the test fixture as the best simulation of flight conditions.

Panel separation.- One partial and two total separations of sandwich panels were achieved in the five tests. Either of the total separations shown in figures V-6(a) and V-6(b) was complete enough to satisfy the requirements for this simulation. The partial separation of figure V-6(c) did not duplicate the separation known to have occurred in flight.

Pressure distributions.- The separation of sandwich panel HS-2 was obtained with the pressure loading of figure V-5(a) and can be explained by considering the pressure-time history in sketch V(a) based on the internal flow model and calculations of appendix B. The sketch shows that the oxygen shelf space is pressurized in about 20 milliseconds whereas pressure in the other compartments builds up more slowly. However, the fuel cell shelf space approaches equilibrium with the oxygen shelf space much sooner than the hydrogen shelf spaces do. These effects result in highly nonuniform initial loadings on the panel that become more and more uniform as the test progresses. The NASTRAN calculations have indicated that the peak uniform pressure for edge failure is only about 75 percent of peak pressure at failure, if just the oxygen shelf space is pressurized. Thus, pressures on panel HS-2 peaked and held constant in the oxygen shelf

(a) Panel DM-6.   (b) Panel DM-7.   (c) Panel DM-10.
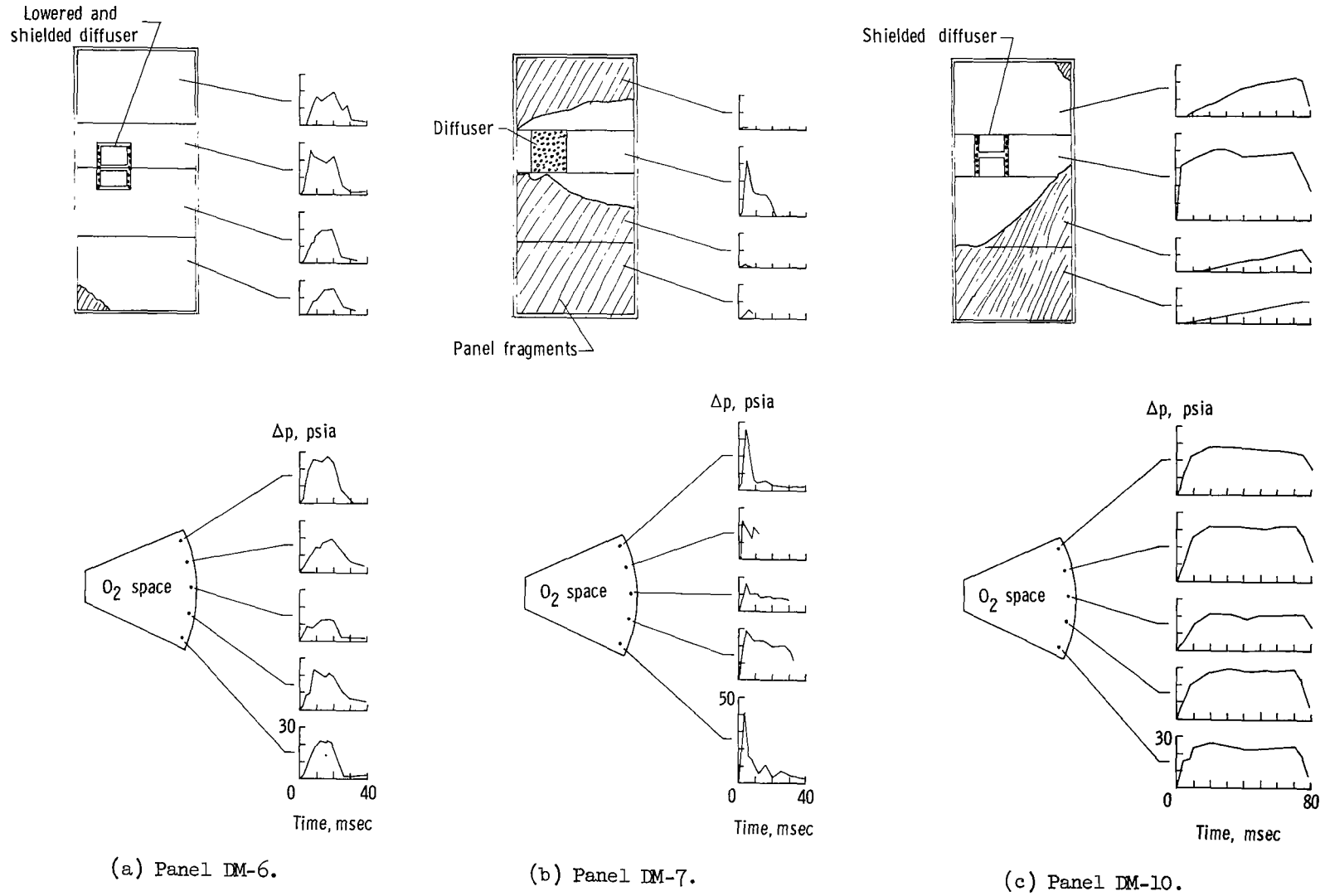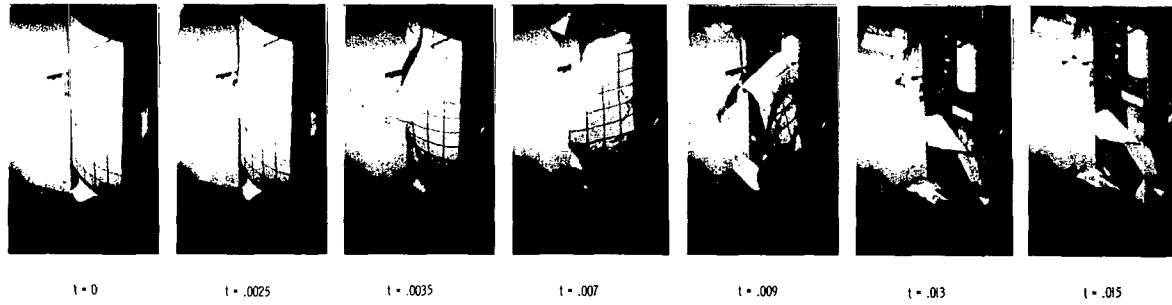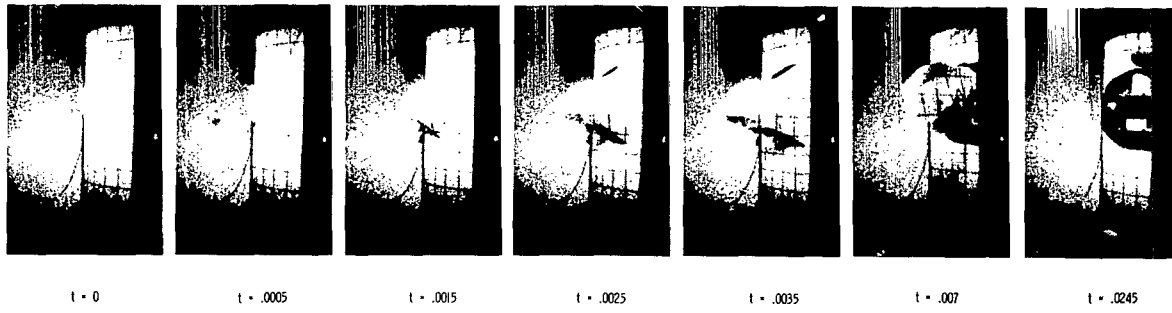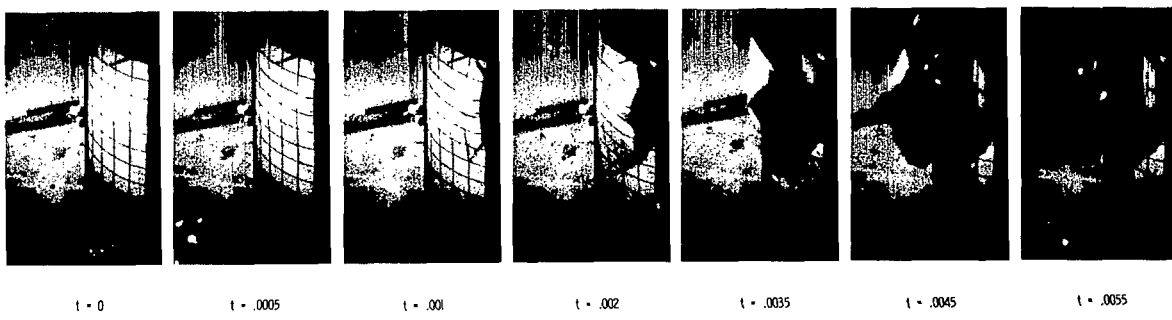
Figure V-3.- Pressure time histories of isotropic panels in vacuum. (t is the time from initial pressure release.)

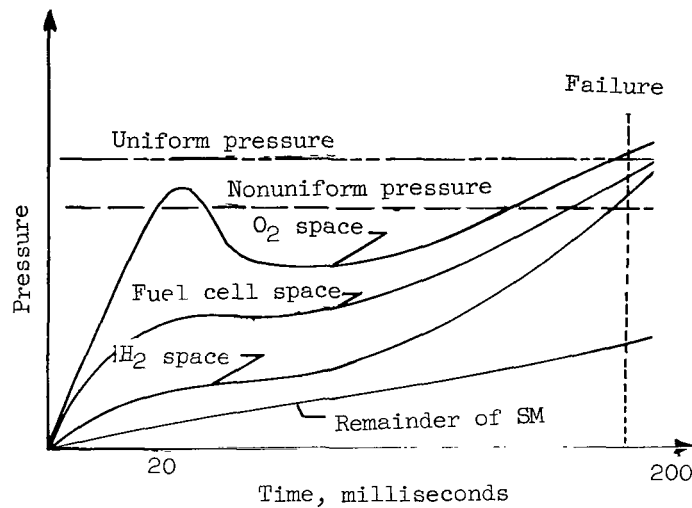t = 0 t = .0025 t = .0035 t = .007 t = .009 t = .013 t = .015

(a) Panel DM-6.

t = 0 t = .0005 t = .0015 t = .0025 t = .0035 t = .007 t = .0245

(b) Panel DM-7.

t = 0 t = .0005 t = .001 t = .002 t = .0035 t = .0045 t = .0055

(c) Panel DM-10.

L-70-4777

Figure V-4.- Sequential failure of isotropic panels in vacuum. (t is the time from first observed failure.)

Sketch V(a).- Typical pressure time history.

space below the pressure required for failure with nonuniform loading. Meanwhile, pressures built up in the other shelf spaces until they finally reached nearly uniform distribution of sufficient magnitude for separation after 190 milliseconds.

Separation was not achieved on panel HS-1 although it was pressurized with a time history similar to that of panel HS-2. A smaller orifice from the source was used and peak pressures were probably lower, although no data were obtained on this particular test. The pressure predictions for these cases in appendix B show panel HS-1 peak pressures about 10 psi below panel HS-2 peak pressures. Together, these two tests have established a boundary for separation of sandwich panels with uniform pressure distributions. They also established lower bounds on the nonuniform pressures required for separation during their initial pressure build-up in the oxygen shelf space.

Panel HS-3 was tested by use of source characteristics that produced very high pressures in the oxygen shelf space (over 50 psi) during the initial pressure build-up. Total separation occurred after 20 milliseconds, while the pressure distribution was still highly nonuniform (as shown in fig. V-5(b)). However, no separation was obtained when panel HS-4 was tested with a slightly smaller orifice to reduce peak pressures. Thus, these two tests established a separation boundary for nonuniform pressure loadings. Pressure time histories for the two cases are compared in figure V-8. Predictions from the mathematical model for both panels are shown in appendix B. The peak pressures in the oxygen shelf space that produce separation with nonuniform loading (HS-3) are 10 to 15 psi greater than the case without separation (HS-4).

A special test on panel HS-5 repeated all conditions for the test on panel HS-3, but with the pressure source diffuser removed. Gas from the source was allowed to expand

directly upward into the oxygen shelf space. The removal of the diffuser resulted in slightly more rapid pressure rise in the upper shelf spaces of bay 4 (shown in fig. V-5(c)). Partial panel separation occurred over these spaces before enough pressure could be built up in the lower shelf spaces to complete panel separation.

Failure mechanisms.- The separation of sandwich panels in a vacuum environment is shown by the photographic sequences of figure V-6. The separation behavior under uniform pressure loading (panel HS-2) appears in figure V-6(a). Failure started at the edge of the oxygen shelf space by pullthrough of the edge bolts through the outer face sheet of the sandwich panel. Very rapid tear-out along three edges followed, primarily by tension in the face sheets and tearing of the core material from the z-stiffener along the edge. The panel then rotated like a door and separated from the test fixture in one piece.

Nonuniform loading of a sandwich panel led to the failure shown in figure V-6(b) for panel HS-3. Initial failure was at the panel edge near the fuel cell shelf. Tear-out along one edge and the top followed rapidly as in the previous separation. However, the edge tear stopped before reaching the bottom and became a diagonal tear that left the lower third of the panel attached to the fixture. The upper two-thirds of the panel rotated door-like and separated. Finally, a vertical tear propagated along a doubler through the center of the remaining fragment, the bottom tore away, and rapid rotation separated the remnants in two pieces.

The partial separation of panel HS-5 (fig. V-6(c)) was almost identical to the first part of the separation of panel HS-3 (fig. V-6(b)). However, the final tear that removed the lower third of panel HS-3 did not occur.

The details of the edge separation of the sandwich panels appear in figure V-7(b). Failure by face-sheet tension and core debonding from the z-stiffener are apparent over most of the perimeter. However, because of the very high inertia loads during the door-opening postfailure action, the simulated radial beam cap failed in bending along the "hinge" side of the failure. These failure details also differ considerably from those of the isotropic panels because of the differences in construction, local stiffness, and postfailure behavior.

Correlation With Flight

Tests with sandwich panels more closely simulate flight conditions than tests with isotropic panels because of panel stiffness properties, internal flow configuration, initial failure characteristics, and postfailure separation behavior. The separation behavior of sandwich panel HS-3 (fig. V-6(b)) is also believed to be more representative of flight than the separation behavior of panel HS-2 (fig. V-6(a)) for two reasons: First, although panel HS-2 was tested with scaled internal venting between the compartments of bay 4

42

Δp, psia

O₂ space

30

0   100   200

Time, msec

(a) Panel HS-2.

Shielded diffuser

Panel fragments

Δp, psia

O₂ space

50

0   40

Time, msec

(b) Panel HS-3.

Direct blast

Δp, psia
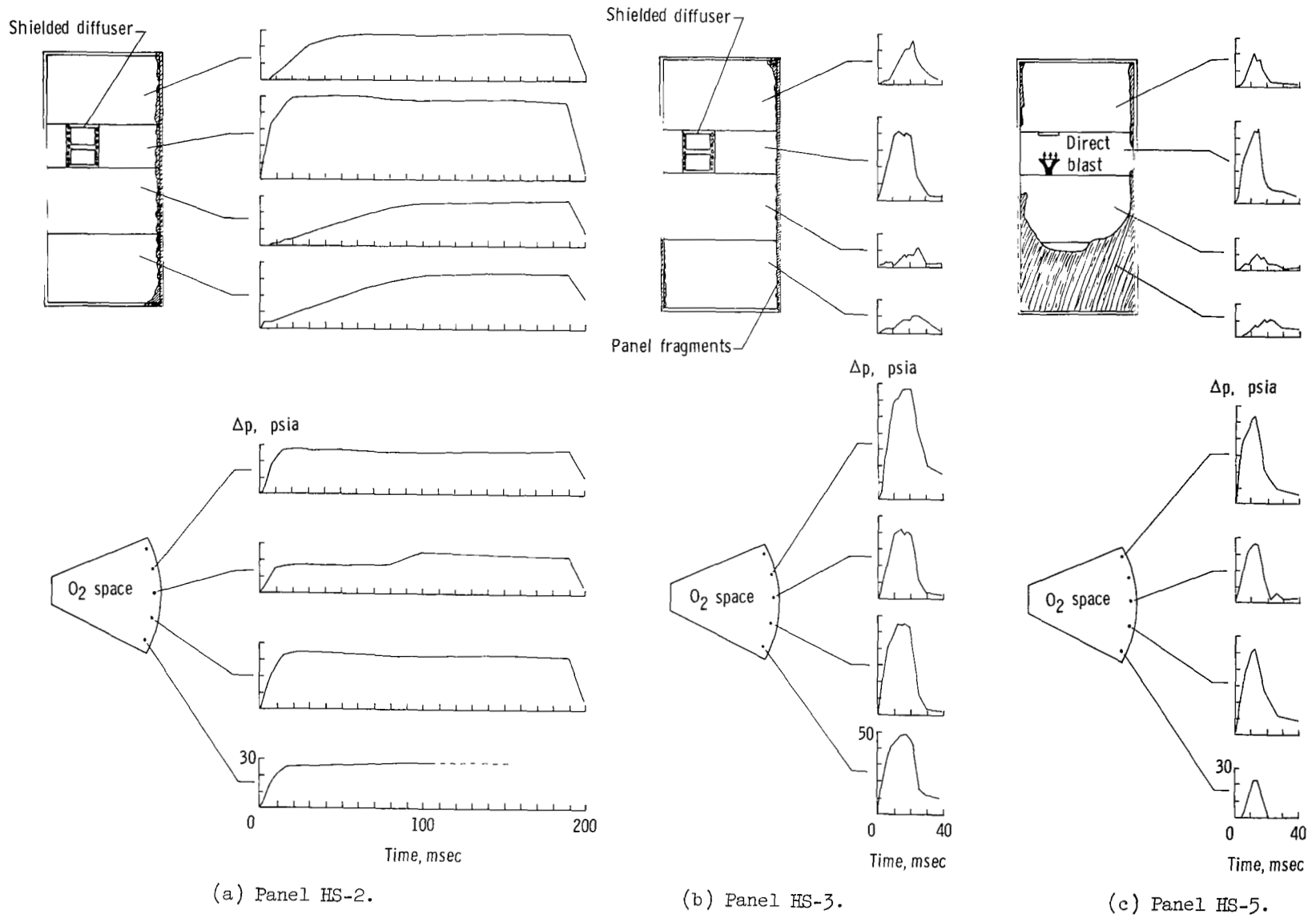
O₂ space

30

0   40

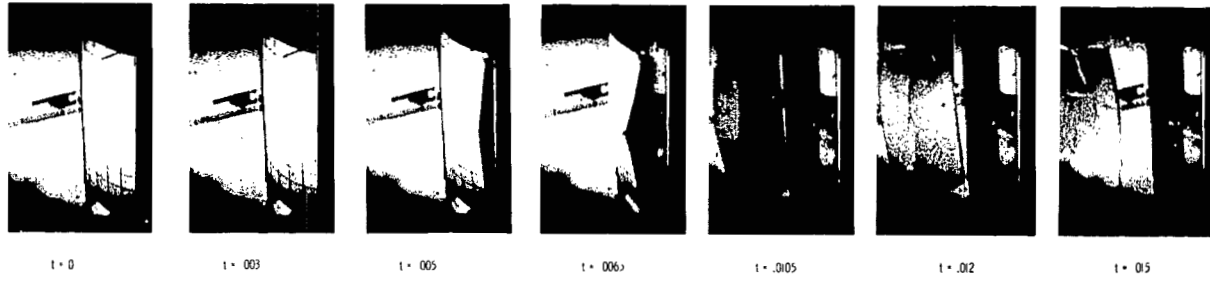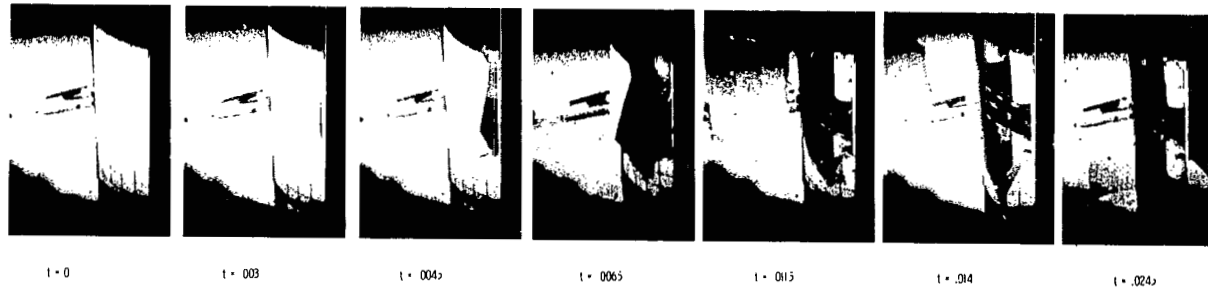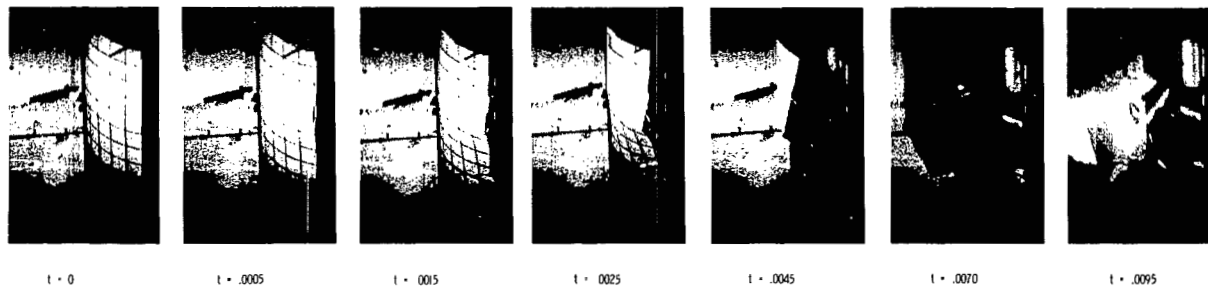Time, msec

(c) Panel HS-5.

Figure V-5.- Pressure time histories of sandwich panels in vacuum. (t is the time from initial pressure release.)
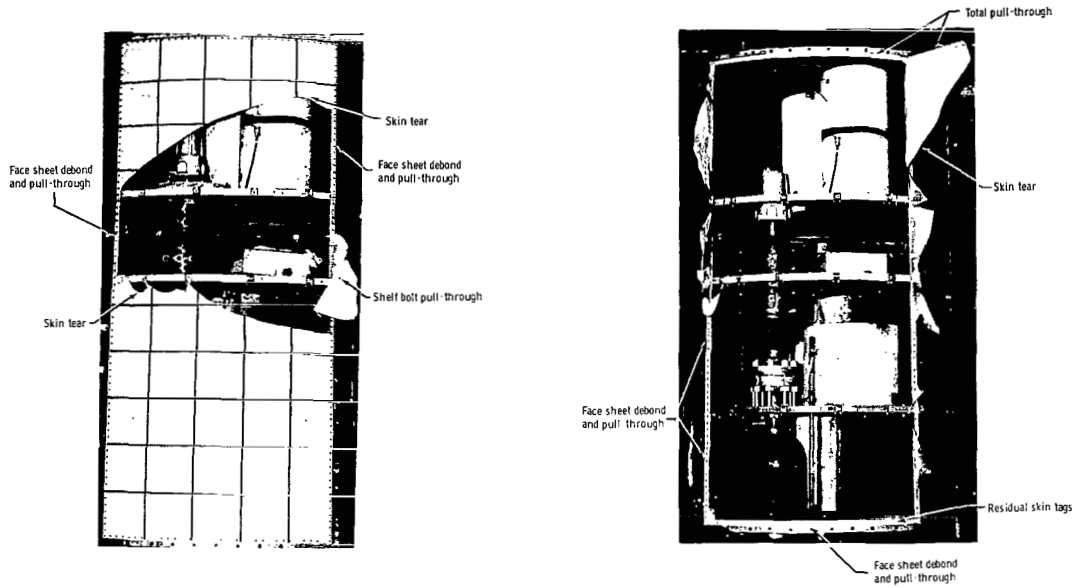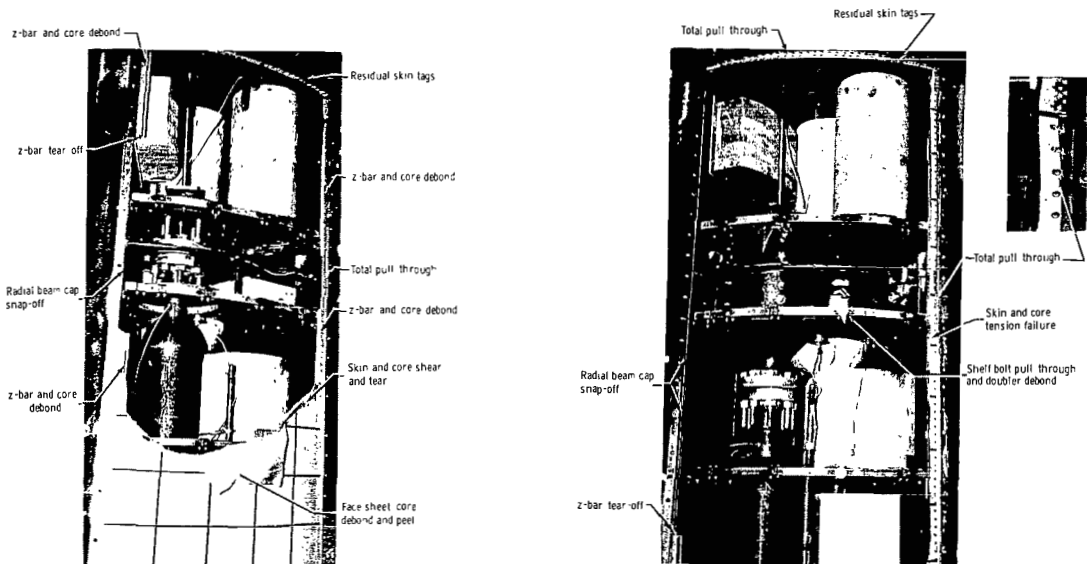
(a) Panel HS-2.

(b) Panel HS-3.

(c) Panel HS-5.

L-70-4778

Figure V-6.- Sequential failure of sandwich panels in vacuum. (t is the time from first observed failure.)

Skin tear

Face sheet debond
and pull-through

Face sheet debond
and pull-through

Skin tear

Shelf bolt pull-through

Total pull-through

Skin tear

Face sheet debond
and pull-through

Residual skin tags

Face sheet debond
and pull-through

(a) Isotropic panels.

z-bar and core debond

Residual skin tags

z-bar tear off

z-bar and core debond

Radial beam cap
snap-off

Total pull-through

z-bar and core debond

z-bar and core
debond

Skin and core shear
and tear

Face sheet core
debond and peel

Total pull through

Residual skin tags

Radial beam cap
snap-off

Total pull through

Skin and core
tension failure

Shelf bolt pull through
and doubler debond

z-bar tear-off

L-70-4779

(b) Sandwich panels.

Figure V-7.- Typical edge failures for half-scale panels.

44

Figure V-8.- Comparison of experimental pressure time histories for panels HS-3 which separated and HS-4 which did not separate.

and the service module tunnel, the rest of the service module free volume had been closed. In the HS-3 panel test, this vent area had been opened to a realistic scaled value of 60 square inches. Second, the slow pressure build-up before separation of panel HS-2 allowed the pressure of the service module tunnel to rise well above the 10-psi limitation required to prevent separation of the command and service modules. However, pressurization leading to panel HS-3 separation was so rapid (20 milliseconds) that pressure in most of the service module tunnel remained below the 10-psi limit. The test pressurization corresponded to a spacecraft pressurization time history that would peak at over 40 psi in the oxygen shelf space in 40 milliseconds.

The relatively high pressure in the fuel cell shelf space during the test of sandwich panel HS-3 leads to a question about the completeness of the internal flow simulation. The fuel cell shelf space, connected by a sizable vent to the oxygen shelf space and pressure source, also had a large vent into the upper part of the service module tunnel that, in turn, was decoupled from the lower part of the service module tunnel by flow restrictions caused by the presence of two large spherical helium tanks. Even though the large volume in the lower tunnel was pressurized slowly, the much smaller upper tunnel pressurization would tend to duplicate that of the fuel cell shelf volume and possibly exceed the 10-psi limitation that prevents command module and service module separation. For the sandwich panel tests, the vent between the tunnel and the simulator of the remainder of the service module free volume had been in the lower tunnel space. In the spacecraft, this vent actually connects through the smaller upper tunnel space and would tend to hold the pressures down. Tests had been completed before this situation was recognized, but the computer model was used to analyze this more representative configuration. Results are presented in appendix C and indicate that, as expected, all interior spacecraft pressures would remain below the 10-psi limit until pressure in the oxygen shelf space reached failure level.

Other factors not considered in the experimental program could affect the correlation of these results with flight. For example, combustion involving escaping oxygen could account for this pressure with small hole sizes in the oxygen bottle. A projectile could be hypothesized that would initiate panel separation at lower pressures. (See "Structural Analysis of Apollo 13 Bay 4 Cover Panel.") Still another possibility is that some small detail omitted in the design and construction of the one-half-scale panel models could alter separation behavior. For instance, the small access doors deleted from the panel conceivably could have a major effect on postfailure behavior, although their effect on initial failure pressure was shown to be small.

VI. CONCLUDING REMARKS

Complete separation of one-half-scale isotropic and sandwich models of the Apollo 13 service module bay 4 cover panel has been demonstrated in a vacuum environment. Complete separation could not be obtained when isotropic panel models were tested in atmosphere because of the retarding effects of air mass and damping on postfailure dynamics.

Separation was demonstrated by use of rapid air pressurization of the oxygen shelf space in the bay 4 compartment. Internal volumes and vent areas of the service module were scaled. Pressure loadings acting on the model cover panels were transient in character, but separations were obtained with both nonuniform and relatively uniform pressure distributions.

Initial failure of both isotropic and sandwich panels occurred under similar loadings and correlated with NASTRAN calculations. These failures were essentially static and were predictable from static-pressure loadings. Dynamic analysis indicated that transient pressure loadings with much shorter characteristic times than those applied in these tests were necessary before significant dynamic overshoot occurred. The final separation from the test fixture, however, was dynamic since inertia loads and postfailure gas dynamics played major roles. The details of the separation of the two kinds of models were also different because of the influence of local stiffness on postfailure dynamics.

Analysis of a sandwich panel with cutouts showed that the presence of the cutout did not substantially alter the failure pressure. However, fracture mechanics analyses showed that a puncture or sharp-edge penetration such as could result from a projectile could substantially lower the failure pressure.

Tests with sandwich panels more closely simulate flight conditions than tests with isotropic panels. The particular test on sandwich panel HS-3 with a nonuniform loading that peaked 20 milliseconds after start of pressurization (40 milliseconds full scale) was most consistent with known flight events. The panel separated in three pieces after an initial tear along the sides that allowed it to open like a door. Inertia loads were the main factor in obtaining complete separation after the initial failure.

A second test was conducted under conditions similar to this simulation but at slightly reduced input pressures. No separation was obtained; therefore, the separation boundary for the most flight-representative pressure time history had been established.

Langley Research Center,
National Aeronautics and Space Administration,
Hampton, Va., September 30, 1970.

Reference

1. Anon.: Report of Apollo 13 Review Board. NASA, 1970.

# APPENDIX A.- TENSILE TESTS ON HALF-SCALE JOINT

By Huey D. Carden and Robert M. Baucom
Langley Research Center

As a part of the Apollo 13 service module panel separation tests, static and dynamic tensile tests were conducted on coupons representative of the one-half-scale isotropic model of the joint between the bay 4 panel and service module attachment to determine the failure mechanism and typical load at failure. This appendix presents typical results from this part of the study.

Static tests consisted of tensile loading of two test coupons at a loading rate of 1000 lb/in. to failure. The two coupons (numbered 1 and 2 and shown in fig. A-1) indicate the type of failure under static tensile load. Both coupons failed by edge pullout behind the two screws. The loads at failure were 1725 lb and 1770 lb for coupons 1 and 2, respectively.

Six coupons were shock loaded to initiate failure. The coupons were suspended from a mounting fixture attached to an impact table. The free end of the coupon was loaded with a relatively large weight. The input of a one-half-sine shock pulse with a time duration of approximately 6 milliseconds as well as the load developed in the coupons were monitored. Typical results for a shock loading test are presented in figure A-2. The input shock load (inverted top trace) and the coupon load response are shown in figure A-2(a) and the resulting failure of the test coupon is shown in figure A-2(b). The failure mechanism for the shock loading tests was also edge pullout from behind the steel screws. The load at failure during the shock tests ranged from 1660 lb to 1720 lb and compares favorably with the average static load of 1750 lb.
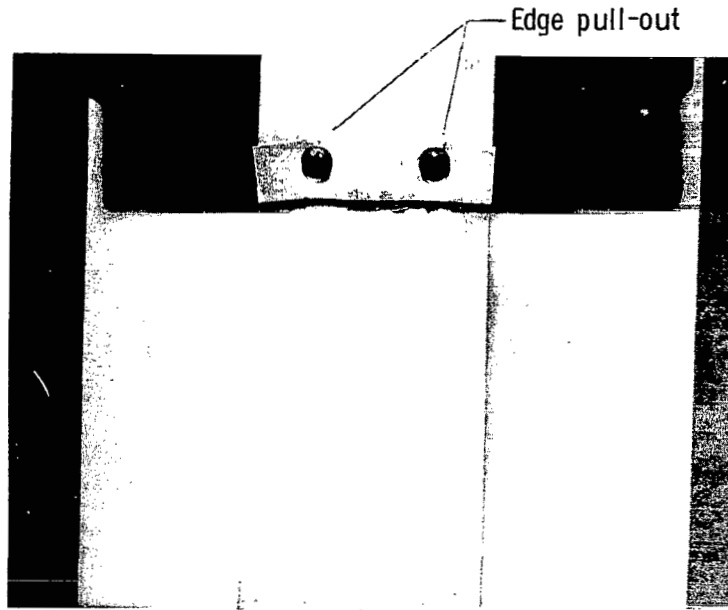
(a) Test coupon 1. Edge pull-out failure load, 1725 lb.
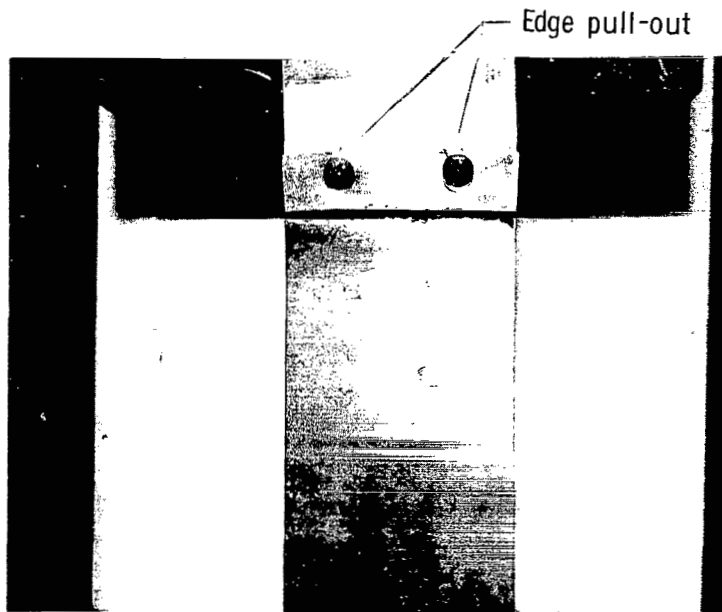
L-70-4780

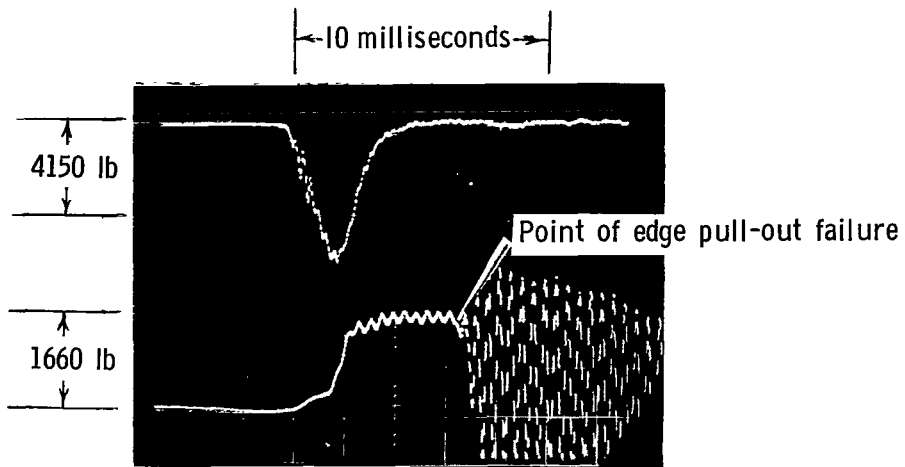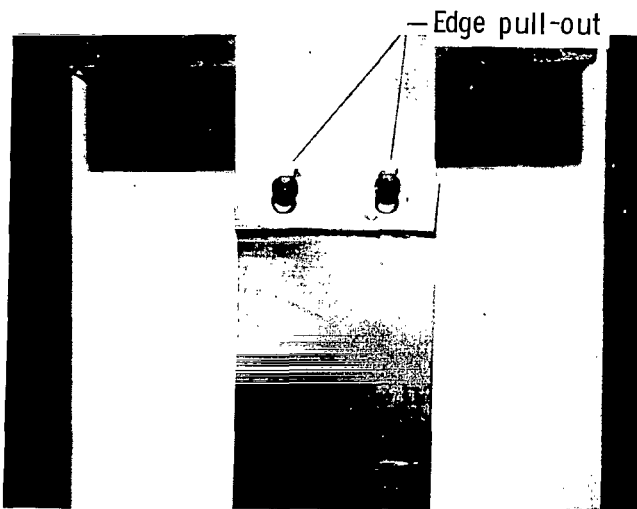(b) Test coupon 2. Edge pull-out failure load, 1770 lb.

Figure A-1.- Static tensile test coupons of simulated half-scale
attachment of panel to service module radial beam cap.

(a) Top trace, input pulse (inverted). Bottom trace, coupon load response.

L-70-4781
(b) Test coupon 5. Edge pull-out failure load, 1660 lb.

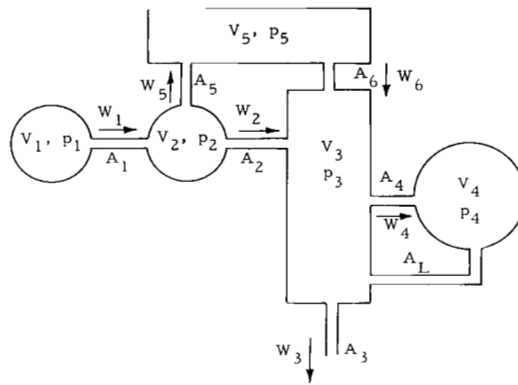Figure A-2.- Dynamic tensile test coupon of simulated half-scale attachment of panel to service module radial beam cap.

APPENDIX B.- CALCULATION OF PRESSURES IN

HALF-SCALE BAY 4 VOLUMES

By Grayson V. Dixon and Jean P. Mason
Langley Research Center

This appendix presents the basic model and system equations used in calculating the pressure time histories in the half-scale bay 4 test fixture with air as the pressurizing gas. The basic model consists of a pressurization source feeding into a set of interconnected volumes designated V_n. (See fig. B-1.) These volumes represent the

Description	Volume designation	Volume, ft^3	Area designation	Area, in^2
Pressure source	V_1	1.0	A_1	(*)
O_2 shelf space	V_2	3.2	A_2	58
Bottom of tunnel and	V_3	28	A_3	17.2
H$_2$ shelf spaces			A_4	(*)
Other SM free volume	V_4	75	A_5	39
Top of tunnel and	V_5	7.3	A_6	16
fuel cell space			A_L	20

*Variable.

Figure B-1.- Areas and volumes for air simulation.

various compartments inside the test fixture. The volumes are vented to each other and to external space through orifices with areas designated A_n. Values for the various V_n and A_n are shown in tabular form in figure B-1. The equations describing the system have been programed for solution on a digital computer.

Volumes and areas used in the machine simulation were in part measured values and in part effective values deduced from comparisons of computed and measured pressure time histories. Volumes V_2, V_4, and V_5 are measured values as are areas A_1

and A_4; however, volume V_3 is larger than its measured value. The effective accumulator volume for the machine calculations was reduced approximately 20 percent from its true water volume to match test results. Gas compressibility, Joules-Thompson effects, and polytropic expansion of the air in the accumulator justify this reduction. Comparison of machine results with test results showed an effective leakage area between volume V_3 and V_4 of approximately 20 in^2. Therefore, a constant leakage area A_L of 20 in^2 was used in all computer calculations. Area A_6 is an effective area deduced from comparison of machine calculations with test pressure time histories. Areas A_2 and A_5 are larger than their measured values in order to give the best match of computer results with tests. Panel distortion before failure (allowing increased venting from the O_2 shelf space to the fuel cell space V_5 and the H_2 shelf spaces V_3) would account for this increase in areas A_2 and A_5. Area A_3 is larger than its measured value to account for leakage.

System Equations

Equations for airflow and pressure were written for the various orifices and volumes. Equations for the airflow and pressure in the O_2 shelf are as follows (T is in $^\circ$R):

$$W_1 = \frac{0.532 A_1 p_1}{\sqrt{T}} \tag{B1}$$

$$p_1 = p_{11} - \frac{RT}{144 V_1} \int W_1 dt \tag{B2}$$

$$W_2 = \frac{1.064 A_2 \sqrt{p_3 (p_2 - p_3)}}{\sqrt{T}} \qquad \left(\frac{p_3}{p_2} > 0.528\right) \tag{B3}$$

$$W_2 = \frac{0.532 A_2 p_2}{\sqrt{T}} \qquad \left(\frac{p_3}{p_2} \leqq 0.528\right) \tag{B4}$$

$$W_5 = \frac{1.064 A_5 \sqrt{p_5 (p_2 - p_5)}}{\sqrt{T}} \qquad \left(\frac{p_5}{p_2} > 0.528\right) \tag{B5}$$

$$W_5 = \frac{0.532 A_5 p_2}{\sqrt{T}} \qquad \left(\frac{p_5}{p_2} \leqq 0.528\right) \tag{B6}$$

$$p_2 = p_{2i} + \frac{RT}{144 V_2} \int_0^t \left(W_1 - W_2 - W_5\right) dt \tag{B7}$$

Equations (B1) to (B7) are typical of those employed for the remaining volumes and areas in the simulation. The pressure surrounding the simulation model was taken as zero.

Typical Results

Some typical results from this simulation are presented in figure B-2. The four curves present time histories of the pressure for the oxygen shelf space p_2, the bottom of the tunnel and hydrogen shelf spaces p_3, the remaining service module free volume p_4, and the combined top of tunnel fuel cell shelf space p_5 for various values for the accumulator orifice A_1 and the vent from tunnel to service module A_4. The values used are comparable with those used for test panels HS-1 to HS-4. In all cases p_1 was set at an initial value of 3000 psi. Figure B-2(a) shows the pressure time history of the fixture with a relatively small $\left(A_1 = 0.8 \text{ in}^2\right)$ accumulator orifice which yields a low peak pressure in the oxygen shelf space and slowly increasing pressures in the other bay 4 volumes. The remaining service module volume shows a low magnitude, slowly rising pressure up to 200 milliseconds. No failure was obtained in the test which this calculation simulates (panel HS-1). Figure B-2(b) shows the results of a 50-percent increase in accumulator orifice area and no volume vent area between the tunnel and service module except for the leakage area A_L. As would be expected, a lower rise time and higher initial pressures are seen in the bay 4 volumes along with a lower pressure response of the service module volume. At approximately 200 milliseconds, the pressure is nearly uniform at a value greater than 30 psi. The test which this calculation simulates (HS-3) resulted in panel failure in approximately 200 milliseconds under fairly uniform pressure.

To obtain the curves shown in figure B-2(c), the accumulator orifice area was set at 2.86 in^2 along with a vent area between tunnel and service module of 60 in^2. This value corresponds to the test conditions for panel HS-3. Very high initial pressure (67 psi) in the oxygen shelf space $\left(p_2\right)$ at 20 milliseconds and lower pressures at later times in the other spaces resulted. Experimentally, this panel failed in two stages, the top two-thirds of the panel first followed by blowoff of the lower one-third.

Computer simulation of the pressure-time history from the test conditions set for panel HS-4 yielded the curves shown in figure B-2(d). In this case the accumulator orifice area was set at 2.0 in^2 along with a vent area between the tunnel and service module of 120 in^2. Initial oxygen shelf space pressure reaches 50 psi at 20 milliseconds; however, the other spaces are all below 15 psi at this time. The pressure equalizes in the O_2 and fuel cell spaces $\left(p_2, p_5\right)$ and then decays to approach the system equalization pressure of approximately 20 psi. The test panel HS-4 did not fail.
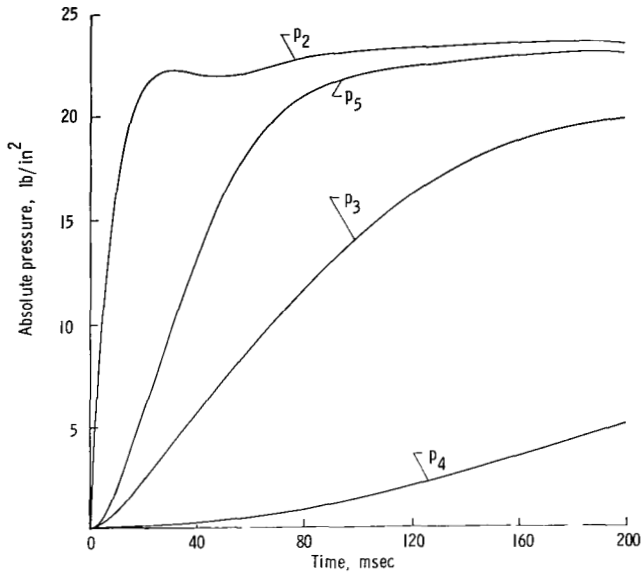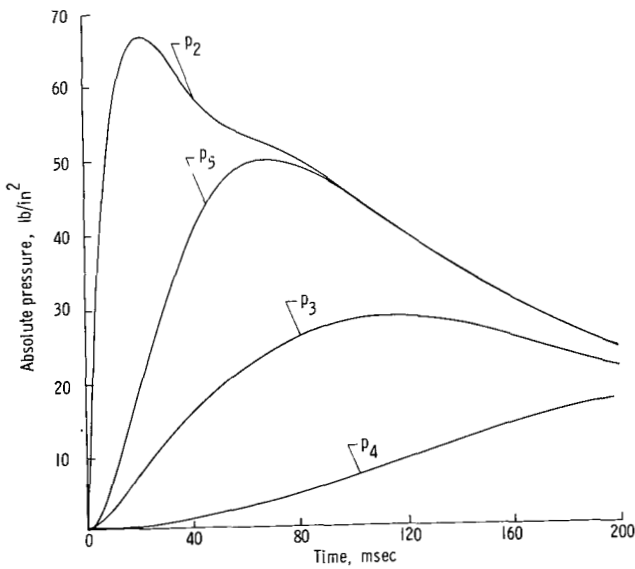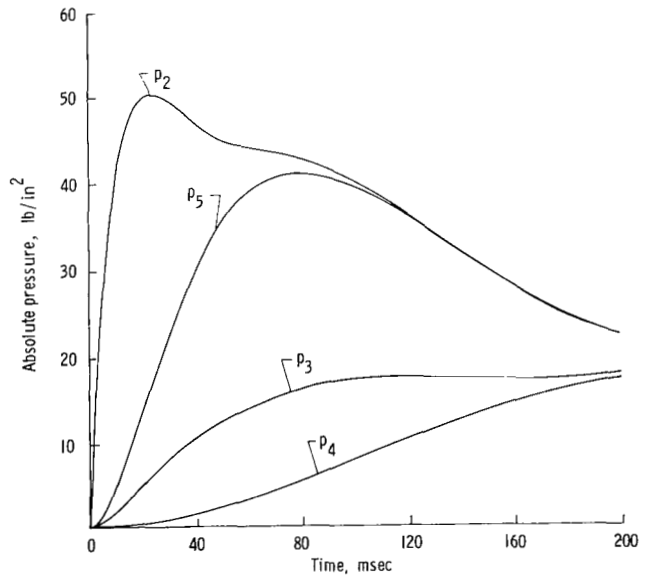
(a) HS-1; $A_1 = 0.8$; $A_4 = 20$.
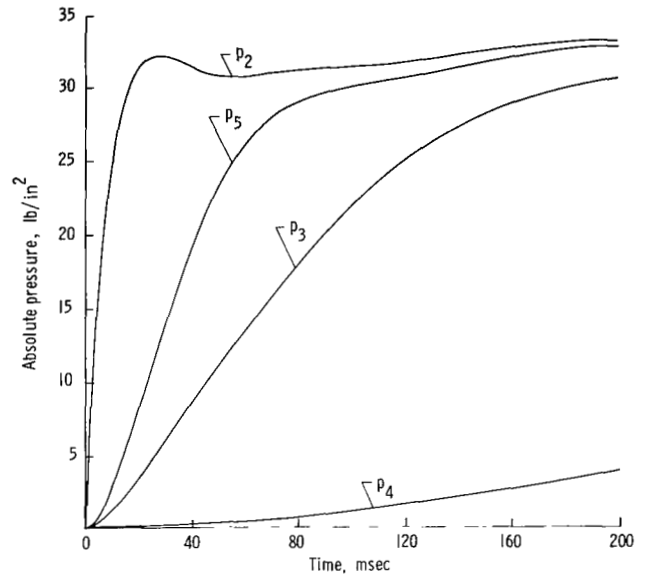
(b) HS-2; $A_1 = 1.2$; $A_4 = 0$.

(c) HS-3; $A_1 = 2.86$; $A_4 = 60$.

(d) HS-4; $A_1 = 2.0$; $A_4 = 120$.

Figure B-2.- Calculated model internal pressure time histories for sandwich panel tests.

APPENDIX C.- CALCULATION OF PRESSURES IN HALF-SCALE

BAY 4 VOLUMES ACCOUNTING FOR VENTS

AT TOP OF SERVICE MODULE TUNNEL

By Grayson V. Dixon and Jean P. Mason
Langley Research Center

In the early phases of the panel separation test program, the two large helium spheres located in the top of the service module tunnel were not simulated and the model tunnel was considered to be a single volume. After these model spheres were installed in the system before testing the sandwich panels, the tunnel could be considered as two volumes vented to each other through the annular area between the spheres and the tunnel wall. Further, all tests were conducted with vent areas from the tunnel to the service module located in the lower tunnel wall. In the flight vehicle, however, considerable vent area is available from the upper tunnel volume to the remaining service module free volume through the space around the upper spherical bulkheads of the four large service propulsion system tanks.
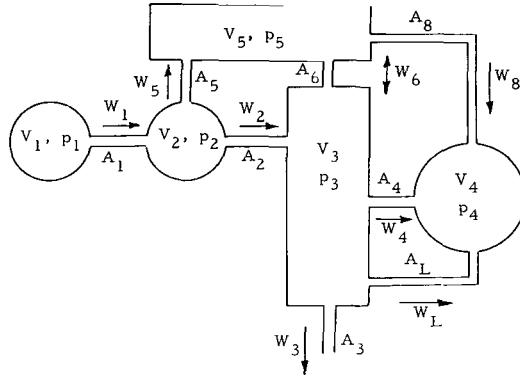
This discrepancy between the venting conditions from the two tunnel volumes to the remainder of the service module free volume has left one aspect of the panel separation problem unresolved. In all the half-scale sandwich panel tests, pressures measured in the fuel cell shelf, which is well vented to the upper tunnel volume, exceeded 10 psi. In the full-scale service module, the top of the tunnel is vented directly to the volume between the service module upper bulkhead and the command module heat-shield face. The structure which holds the two modules together would have failed in tension and the service module and command module would have separated if the pressure in this volume had reached 10 psi during the Apollo 13 anomaly. Since the two modules did not separate, one may deduce that the upper tunnel and fuel cell volume pressures did not reach the 10-psi level.

In order to examine the behavior of the half-scale system with the top of the tunnel having vent properties more closely representative of the flight vehicle, the model described in figure C-1 was analyzed. In this model, the area A_6 represents the constriction in the tunnel due to the presence of the helium spheres; A_8 represents a venting from the top of the tunnel around the service propulsion system bulkheads; and the pressures p_3 and p_5 represent pressures in the bottom and top of the tunnel, respectively.

The calculated pressure time history shown in figure C-2(a) represents a configuration having only the leakage vent A_L between the bottom part of the tunnel and the

service module and having an effective vent area between the top of the tunnel and the service module (A_8) of 80 in^2. In figure C-2(b) the area A_8 is maintained at 80 in^2 and the bottom tunnel vent area (A_4) is set at 60 in^2. In both cases, the oxygen shelf pressure is the same and peaks at about 20 milliseconds to a value near 65 psi, and the


| Description	Volume designation	Volume, ft^3	Area designation	Area, in^2
Pressure source	V_1	1.0	A_1	(*)
O_2 shelf space	V_2	3.2	A_2	58
Bottom of tunnel and	V_3	28	A_3	17.2
H$_2$ shelf spaces			A_4	(*)
Other SM free volume	V_4	75	A_5	39
Top of tunnel and	V_5	7.3	A_6	16
fuel cell space			A_8	(*)
			A_L	20

*Variable.

Figure C-1.- Areas and volumes for air simulation with top of tunnel venting.

two tunnel pressures p_3 and p_5 are virtually the same at this time point. The model used in calculating the curves in figure C-2(c) had values for A_4 and A_8 of 0 and 120 in^2, respectively. In this case, the data show that the O_2 shelf space pressure p_2 is not radically affected by the vent area changes; however, at a time of peak O_2 shelf pressure (20 milliseconds), both of the tunnel pressures are less than 10 psi. It is therefore possible to infer that reasonable vent areas around the forward service propulsion system tank bulkheads could prevent failure of the command module and service module interconnect hardware and yet still permit pressure buildups in the bay 4 area sufficient to induce panel separation.
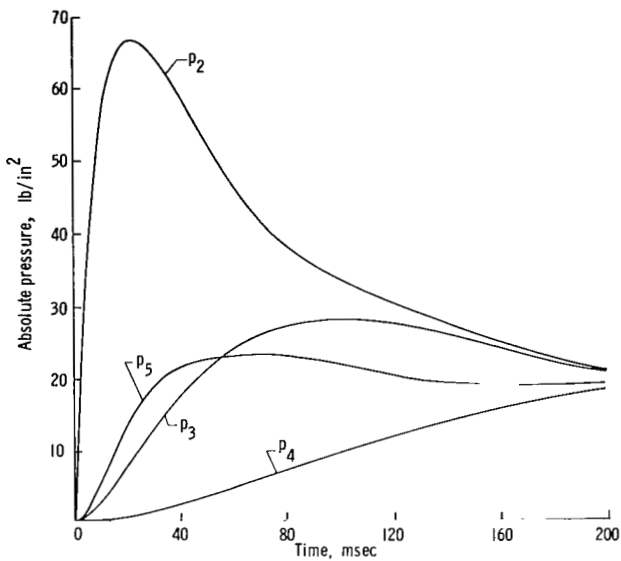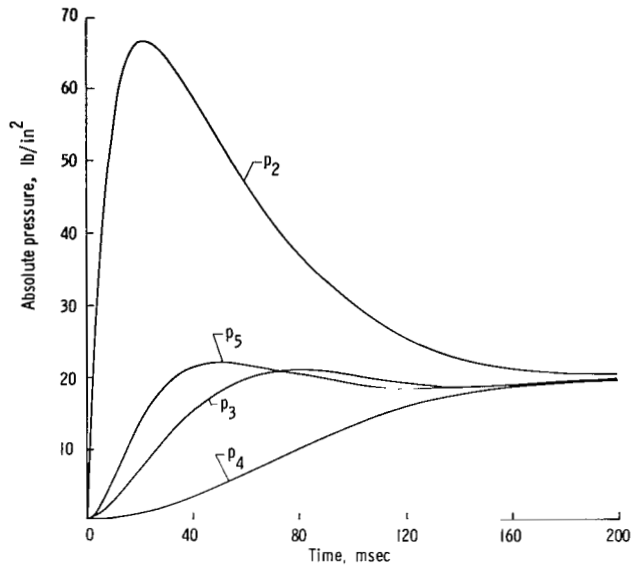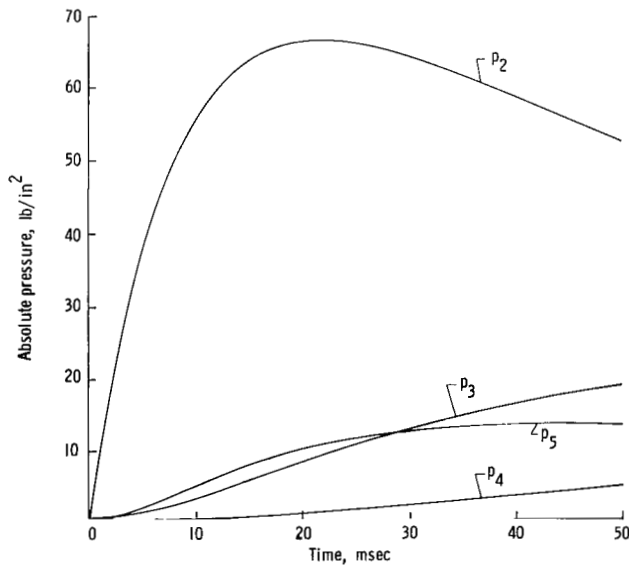
(a) $A_4 = 0$; $A_8 = 80$.

(b) $A_4 = 60$; $A_8 = 80$.

(c) $A_4 = 0$; $A_8 = 120$.

Figure C-2.- Calculated model internal pressure time histories for model with vents at top of tunnel.

"The aeronautical and space activities of the United States shall be conducted so as to contribute . . . to the expansion of human knowledge of phenomena in the atmosphere and space. The Administration shall provide for the widest practicable and appropriate dissemination of information concerning its activities and the results thereof."

— NATIONAL AERONAUTICS AND SPACE ACT OF 1958

NASA SCIENTIFIC AND TECHNICAL PUBLICATIONS

TECHNICAL REPORTS: Scientific and technical information considered important, complete, and a lasting contribution to existing knowledge.

TECHNICAL NOTES: Information less broad in scope but nevertheless of importance as a contribution to existing knowledge.

TECHNICAL MEMORANDUMS: Information receiving limited distribution because of preliminary data, security classification, or other reasons.

CONTRACTOR REPORTS: Scientific and technical information generated under a NASA contract or grant and considered an important contribution to existing knowledge.

TECHNICAL TRANSLATIONS: Information published in a foreign language considered to merit NASA distribution in English.

SPECIAL PUBLICATIONS: Information derived from or of value to NASA activities. Publications include conference proceedings, monographs, data compilations, handbooks, sourcebooks, and special bibliographies.

TECHNOLOGY UTILIZATION PUBLICATIONS: Information on technology used by NASA that may be of particular interest in commercial and other non-aerospace applications. Publications include Tech Briefs, Technology Utilization Reports and Notes, and Technology Surveys.

Details on the availability of these publications may be obtained from:

SCIENTIFIC AND TECHNICAL INFORMATION DIVISION
NATIONAL AERONAUTICS AND SPACE ADMINISTRATION
Washington, D.C. 20546